Agricultural and Forest Meteorology 174–175 (2013) 184–201

Contents lists available at SciVerse ScienceDirect

Agricultural and Forest Meteorology

journal homepage: www.elsevier.com/locate/agrformet

Mapping dry-season tree transpiration of an oak woodland at the catchment scale, using object-attributes derived from satellite imagery and sap flow measurements

J. Leonardo Reyes-Acosta[a,b,*], Maciek W. Lubczynski[a]

[a] Faculty of Geo-Information Science and Earth Observation (ITC), University of Twente, Henegelosestraat 99, 7500AE Enschede, The Netherlands
[b] Centro Hispano Luso de Investigaciones Agrarias (CIALE), Universidad de Salamanca, Calle del Duero, 12, 37185 Villamayor, Spain

ARTICLE INFO

Article history:
Received 14 September 2012
Received in revised form 13 February 2013
Accepted 16 February 2013

Keywords:
Sap-flow scaling-up
Transpiration
HFD
Quercus ilex
Quercus pyrenaica
Semi-arid open-forest

ABSTRACT

Tree transpiration is an important plant-physiological process that influences the water cycle, thereby influencing ecosystems and even the quantity of available water resources. However, direct tree-transpiration measurements, particularly at large spatial scales, are still rare, due to the complexities associated with natural ecosystems. In this study we describe a scaling-up method for quantifying dry-season tree transpiration (T_c) of the Sardón catchment, located in Central-Western Spain, 50 km west of Salamanca. The method is applied to an oak woodland in that catchment which is dominated by two tree species: evergreen *Quercus ilex* and deciduous *Quercus pyrenaica* (*Q.i.* and *Q.p.*, respectively). The method comprises five complementary steps: (a) sap-flux density (J_p) measurement; (b) definition of biometric-upscaling functions; (c) spatial scaling-up of tree transpiration using high-resolution remote-sensing-derived object attributes (50–60 cm per pixel); (d) modelling of dry-season temporal sap-flow variability; and (e) an assessment of the robustness/uncertainty of the method. The proposed method was applied to assess dry-season tree transpiration, however if there is appropriate sap flow data available, it can also be applied during any season of the year. The application of the proposed method to map tree transpiration in the Sardón catchment resulted in a mean J_p = 58.4 cm^3 cm^{-2} day^{-1} for *Q.p.*, characterized by tree density of 19 trees ha^{-1}, and a mean J_p = 37.1 cm^3 cm^{-2} day^{-1} for *Q.i.*, characterized by tree density of 4 trees ha^{-1}. The J_p data varied as dependent on the weather conditions and not on the change of soil moisture. The mean normalised tree transpiration (T_t) estimated per species, was also higher for *Q.p.* (1.19 mm day^{-1} ±8%) than for *Q.i.* (0.83 mm day^{-1} ±25%) trees. The remote-sensing scaling up of tree transpiration for the Sardón catchment resulted in a low mean dry-season T_c = 0.045 mm day^{-1} (±1%) typical for water limited environments with sparse tree coverage (average ≈7%). In that T_c, *Q.p.* represented 79%, whereas *Q.i.* 21%. The dry-season T_c varied spatially at 1 ha resolution but barely temporally throughout the dry season. The obtained T_c maps can be readily used as input for distributed models in water resources and land management decision-making.

1. Introduction

Assessment of tree transpiration between and within different biophysical scales in the soil–plant–atmosphere continuum is an appropriate approach for understanding the role vegetation plays in hydrology (Lubczynski, 2000, 2009; David et al., 2004; Hernández-Santana et al., 2009). Accurate quantification of transpiration dynamics is crucial in fields such as water resources assessment (Lubczynski, 2000, 2009), forest management (Brown et al., 2005), agricultural practices (Lu et al., 2002), and for acquiring a better understanding of climate change (Martínez-Vilalta et al., 2002), to mention just a few. Diverse approaches to measure transpiration *in situ* (Čermák et al., 1982; David et al., 2007; Devitt et al., 1993; Hernández-Santana et al., 2008a) and/or indirectly (Calder, 1978; Caspari et al., 1993; Moore et al., 2008; Verbeeck et al., 2007) have been reported in the literature. The challenge still remains, however, to represent transpiration at higher, for example, catchment scales.

Typically, the tree transpiration studies have attempted to quantify transpiration of stands of pristine, semi-natural or cultivated forests (Čermák and Kučera, 1990; Hatton and Wu, 1995; Granier et al., 1996; Vertessy et al., 1997; Köstner et al., 1998; Wullschleger et al., 1998; Lundblad and Lindroth, 2002; Ford et al., 2007; Nagler

* Corresponding author at: Faculty of Geo-Information Science and Earth Observation (ITC), University of Twente, Henegelosestraat 99, 7500AE Enschede, The Netherlands.
E-mail addresses: l_reyes@itc.nl (J.L. Reyes-Acosta), Lubczynski@itc.nl (M.W. Lubczynski).

0168-1923/$ – see front matter © 2013 Elsevier B.V. All rights reserved.
http://dx.doi.org/10.1016/j.agrformet.2013.02.012

et al., 2007), the vegetation cover of which was closed and dominated by tree canopies. In such stands, the classical procedure is to establish species-specific, mathematical functions, relating sap flow with the stem size based on some few measurements of the selected trees. Such functions allow the inference of transpiration for the trees not measured (Čermák et al., 2004). Such approach can be technically complicated and thus of limited use for large scale studies of sparse forests in water-limited environments (WLEs), such as Mediterranean dehesas in Spain (Lubczynski and Gurwin, 2005; Reyes-Acosta and Lubczynski, 2012) or the savannahs of the Kalahari (Kimani et al., 2007; Chavarro et al., 2009). Those forests are characterized by highly variable tree sizes and sparsely located trees (distance between trees can be >10 m), which makes direct data collection and the establishment of a robust mathematical relations between biometric characteristics and sap flow difficult, and the acquisition of all the stem characteristics necessary for scaling up large areas, practically impossible. Therefore a reliable alternative is to use remote sensing for scaling tree sap flow measurements.

The remote sensing based scaling up of tree sap flow measurements has been demonstrated already by Čermák and Kučera (1990) who argued that such scaling up procedure is a good alternative for estimating tree transpiration at high spatial scales. They described an approach focused on determining a mathematical relation between sap flow and reflectance of the foliage of canopies in the near-infrared region of the spectrum (band 7 from multispectral images acquired with a double lens reflex camera).

More recently, Boegh et al. (1999), Nagler et al. (2007), Murray et al. (2009) and Cristóbal et al. (2011) have further explored the possibilities of using remotely sensed images to quantify evapotranspiration at large scales (*ET*) by using vegetation indices, for example the Normalized Difference Vegetation Index (NDVI) and the Enhanced Vegetation Index (EVI). Boegh et al. (1999) calculated these indices using Landsat-TM and Spot images (20 m spatial resolution). Nagler et al. (2007) and Murray et al. (2009) used images from the Moderate Resolution Imaging Spectrometer (MODIS) (250 m spatial resolution), whereas Cristóbal et al. (2011) used a combination of both. Boegh et al. (1999) proposed that the status of such indices can be mathematically related to transpiration (*T*), while Nagler et al. (2007), Murray et al. (2009), Cristóbal et al. (2011) have argued that they can be related to *ET*. Each of these five studies, however, is based on the electromagnetic properties of the vegetation and not on the attributes of the objects in the images: size, shape, colour, and compactness, for example. Furthermore, the spatial resolution of these Landsat-TM, Spot and MODIS images do not allow the definition of individual canopies. In addition, the approach using MODIS cannot discriminate yet between evaporation and transpiration; and the associated errors are 20–30% (Nagler et al., 2007; Murray et al., 2009; Cristóbal et al., 2011). All these factors reduce the applicability of vegetation indexes derived from electromagnetic properties to quantify *T* in sparse vegetation areas of WLEs.

As the spatial resolution of satellite-based products has significantly increased during the last decade, high-resolution remotely sensed images are now readily available for detecting object attributes of single canopies, facilitating the mapping of transpiration in large catchment scales. The remote-sensing method of scaling-up sap flow measurements for transpiration mapping is especially suitable for quantifying transpiration of sparse vegetation composed of a small amount of tree species (Lubczynski, 2009), so that the probability of misclassification of tree species is minimized (Kimani et al., 2007; Lubczynski, 2009; Chavarro et al., 2009). The first attempt to use object attributes from high-spatial resolution remotely sensed images to scale up sap flow measurements in the Kalahari Desert was reported by Chavarro et al. (2009). They demonstrated that the main advantage of scaling-up single-tree sap flow measurements to large scale estimates using high-resolution images, was the higher accuracy and resolution of the tree transpiration estimates (tree level). In our study, we have further developed and evaluated this approach by: (i) correlating canopy areas defined from satellite imageries with sapwood areas and not with sap flow measurements following Lubczynski (2009); (ii) including radial and azimuthal sap flux density measurements (J_{pi}) in the scaling-up process after Reyes-Acosta and Lubczynski (2012), and by (iii) evaluating its uncertainty.

The aims of our study were: (a) to scale-up tree transpiration estimates in mm day^{-1}, to a grid of 1 ha resolution, based on in-situ sap flow measurements of individual evergreen (*Quercus ilex* subsp. *ballota*) and deciduous (*Quercus pyrenaica* Wild) oak trees (*Q.i.* and *Q.p.*, respectively) to represent spatial variability of tree transpiration at the stand and catchment scales; (b) to simulate the temporal variability of sap flow (Q_s) during the dry-season and describe its implications for spatial transpiration estimates; and finally (c) to evaluate the robustness and uncertainties of scaling up transpiration by using attributes derived from identified objects in remotely sensed images.

To our knowledge, this is the first description reported in the literature of tree-transpiration mapping at the catchment scale based on the scaling up of sap flow measurements using object attributes identified in remotely-sensed images. This study is part of a larger hydrological research programme focusing on the spatiotemporal variability of subsurface water fluxes in the Sardón catchment (Central-Western Spain), which is currently being carried out by the Water Resources Department of the Faculty of Geo-information Science and Earth Observation (ITC) of the University of Twente.

2. Materials and methods

The tree transpiration of the Sardón catchment was quantified spatially by combining two complementary steps: (a) sap flow measurement, and (b) the spatial scaling up of the sapwood area of individual trees using object attributes identified in high-resolution remotely sensed images. These steps are described in the following sections.

In our study we have focused on the dry season because sap flow data collected during this period is typically the most relevant for (and demanded by) hydrologists (Lubczynski, 2009). Therefore, in this study, the dry season conditions were analyzed and standardized as follows: absence of rainfall, continuous periods of clear-sky days, daily peaks of solar radiation >700 W m^{-2}, and maximum daily vapour pressure deficits >1.5 kPa. The sap flow measurements and tree transpiration maps obtained in this study are assumed to be valid under such standardized conditions.

2.1. Study area

This study was developed in the Sardón catchment ≈80 km^2 (Fig. 1), which is characterized by low population density and, with that, equally low levels of human impact (Lubczynski and Gurwin, 2005). The climate of the Sardón study area is semi-arid, with a mean rainfall of ≈500 mm yr^{-1} (Lubczynski and Gurwin, 2005). The warmest and the driest months are July and August, with an average temperature of 22 °C, potential evapotranspiration (PET) of 5 mm day^{-1} calculated from the Penman–Monteith equation (Allen et al., 1998) and rainfall <3 mm month^{-1} (Lubczynski and Gurwin, 2005). The bare soil evaporation during dry season is ≈0.55 mm day^{-1}, as estimated by a liquid and vapour water flow model calibrated against soil moisture measurements (Balugani et al., 2011).

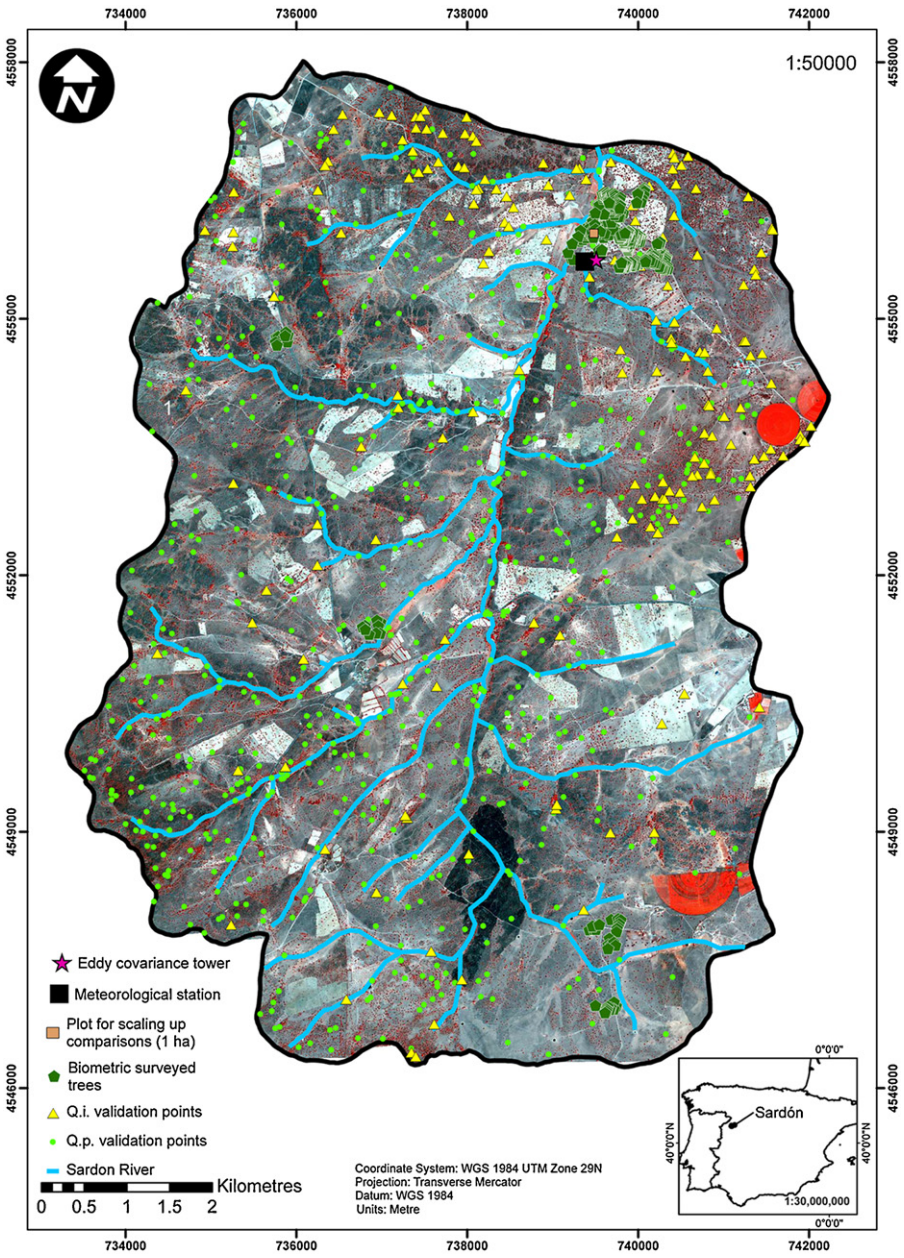

Fig. 1. "*QuickBird*" image of 60 cm resolution (pan-sharpened) in false colour composition with bands 4–2–1 acquired on 9th August 2009 for the Sardón catchment. The vegetation is highlighted in red by the near-infrared band 4 (the red semi-circles are grasses cultivated for pasture). Additional spatial features indicate the locations of data acquisition (meteorological data, tree-biometrics, etc.) and the main river streams are indicated in blue. (For interpretation of the references to color in this figure legend, the reader is referred to the web version of the article.)

The Sardón catchment is composed of massive, fractured and weathered granites with inclusions of schists and gneisses. The superficial, weathered, unconsolidated material is only a few metres thick and is widely intercalated by solid granite outcrops. The water-table is hydraulically connected to intermittent streams in valleys and at topographic elevations rests some few metres below the ground surface. The study area is a woodland with scattered patches of woody-shrub vegetation (*Cytisus scoparius*, also known as Scotch Broom) and a semi-natural open forest containing two dominant tree species: the evergreen oak *Quercus ilex* (*Q.i.*) subsp. *ballota* Desf. (Samp.) and the broad-leafed deciduous oak *Quercus pyrenaica* (*Q.p.*) wild. *Q.i.* trees have small sclerified leaves and are well adapted to drought stress (Manes et al., 2006), whereas *Q.p.* trees have broad lobulated leaves and grow better in sub-humid/humid environments, although they also tolerate dry conditions (Hernández-Santana et al., 2008b). The understory vegetation in the Sardón catchment is mainly composed of summer-annual grasses that wilt during the dry season, therefore their dry season water uptake was considered negligible in this study.

The climatic conditions of the Sardón catchment during summer are characteristic of a WLE. Sap flow measurement under such WLE conditions is challenging due to the sensitivity of the measurement techniques to a number of potential inaccuracies, summarized in Section 2.3.

2.2. Measurement of biometric characteristics

The biometric characteristics of oak trees in the Sardón area were surveyed for use in the scaling-up process. A full description of the survey design can be found in Reyes-Acosta and Lubczynski (2012). The survey focused on obtaining the biometric

characteristics necessary to define the attributes of the tree population, for example: diameter at breast height (DBH), cross-sectional area of the tree stem, (A_s), ground projected canopy area (A_c) and sapwood area (A_x). These measurements were obtained from 90 *Q.i.* and 84 *Q.p.* trees (see Fig. 1 for their location) and further processed to statistically define the tree-size categories (i.e. structure of the population). In this study the A_x was selected as an appropriate parameter to define the population structure for scaling up transpiration because it has been related to the state of growth of the trees (Gea-Izquierdo et al., 2009) and has a low temporal variability. The A_x scaled parameter was calculated by determining the depth of the sapwood in the stems using two techniques, namely: visual inspection of dyed wood-cores and by measuring depth-wise sap flux densities using the heat field deformation (HFD) method. The corresponding A_c scalar was defined by estimating the projected area of the canopy with a minimum of two transects across the ground demarcated by 90° angles with a clinometer. For further details on the A_x and A_c measuring field-campaign, see Reyes-Acosta and Lubczynski (2012).

2.3. Sap flow measurements

Sap flow measurement (Q_s) is a widely used method for quantifying whole-plant water use (Lu et al., 2004) and can express transpiration fluxes, provided stem storage can be neglected. Q_s measurement consists of separate measurements of sap flux density (J_p) and sapwood (xylem) area A_x (Čermák et al., 2004; Granier, 1985; Lu et al., 2004; Lubczynski, 2009), following Eq. (1):

$$Q_s = J_p \times A_x \quad (1)$$

where J_p is typically expressed in $cm^3\ cm^{-2}\ h^{-1}$ and xylem area (A_x) in cm^2. In this study, Q_s was measured in *Q.i.* and *Q.p.* trees during monitoring campaigns conducted in the summer of 2009 and 2010 using thermal dissipation probes (TDPs) and heat field dissipation (HFD) sensors, as presented in Reyes-Acosta and Lubczynski (2012). Depending on the DBH of each tree, one to three TDPs were used.

The TDP method has been widely used in many studies (Chu et al., 2009; Granier, 1987; Köstner et al., 1998; Lu et al., 2004; Paço et al., 2009; Regalado et al., 2009) and features an empirical but widely tested calibration to relate measured temperature differences between two thermocouples (one heated and the other not) inserted in the sapwood (ΔT in °C) at 10 cm distance, with sap flux density J_p (in $cm^3\ cm^{-2}\ h^{-1}$) (Granier, 1985). The TDP method has a good validation record for oak species (Granier et al., 1994). However, considering that the 2 cm sensing length of the standard TDP probes was not sufficient to cover the entire depth of the investigated oaks (sapwood depth >2 cm), additional radial measurements were necessary to properly quantify sap flow (check Reyes-Acosta and Lubczynski (2012) for the reported sapwood depths larger than 2 cm).

Such measurements were made with HFD sensors (ICT International, Armidale, NSW, Australia). The HFD sensors have 8 measuring points each spaced 1 cm apart, starting at 0.5 cm through 7.5 cm sensing depth. The HFD method determines J_p based on the spatial deformation of a heat field around a linear heater (placed tangentially in the sapwood of the tree being studied), represented by the ratio of the measured temperature differences symmetrically (δT_{sym}) and asymmetrically (δT_{asym}) (Nadezhdina et al., 1998, 2002, 2012). To determine the radial and azimuthal sap-flow variations in the sampled trees, two HFD sensors were used at the same time for two days at opposite azimuths, and then rotated to measure the other opposite azimuths for additional two days. Both species, *Q.i.* and *Q.p.*, presented significant radial variations deeper than 2 cm and also azimuthal variations. More information on the fieldwork setup and on the assessment of the radial and azimuthal variabilities can be found in Reyes-Acosta and Lubczynski (2012).

The objective behind combining the TDP and the HFD methods was to optimise sap flow measurement by taking advantage of the robustness and cost-effectiveness of TDP sensors, and the enhanced xylem-depths resolution of HFD sensors, which unfortunately are of limited use because of their high cost. The applied optimisation allowed handling the three types of common TDP inaccuracies, related to: (1) biases from the influence of natural thermal gradients (NTGs) (Do and Rocheteau, 2002a,b; Lu et al., 2004; Lubczynski et al., 2012; Reyes-Acosta et al., 2012); (2) radial and azimuthal variability of J_p (Nadezhdina et al., 2002; Poyatos et al., 2007); and (3) night-flow in trees and related uncertainty in the assumption of a ΔT_{max} value (Reyes-Acosta and Lubczynski, 2012).

The trees assigned for sap flow measurements were selected by: (1) determining their size category; (2) making sure they had symmetrical stems; and (3) verifying that they did not present any apparent sign of decay (hollow trunks) and/or illness (e.g. presence of infected black tissue in core samples). To properly account for tree-size variability in the population, but with minimum amount of measurements, the TDP and HFD sap flow measurements followed a stratified sampling scheme. The stratified sampling comprised distributing a 10-trees sample between the tree-size categories established from the biometric measurements of A_x and measuring the corresponding J_p for each of those categories. Next the J_p and the sap flux density for the outermost 2 cm of the xylem ($J_{p\,2\,cm}$) were plotted against corresponding A_x as in Fig. 2. In this figure, based on $J_{p\,2\,cm}$, an arbitrary categorization of the sap flux density as dependent on A_x has been made. The assigned $J_{p\,2\,cm}$ categories were as follow: (1) "Small", for *Q.i.* trees trees with $A_x < 300\,cm^2$ and for *Q.p.* with $A_x < 200\,cm^2$; (2) "Medium" for *Q.i.* trees with $300\,cm^2 \leq A_x < 400\,cm^2$ and for *Q.p.* with $200\,cm^2 \leq A_x < 400\,cm^2$; and (3) "large" for both tree species with $A_x \geq 400\,cm^2$.

2.4. Modelling of temporal sap-flow variability

The sap flow data obtained was limited to short campaigns of continuous daily measurements at 10 min intervals during different time periods of the dry season, due to technical and logistics limitations. To be able to provide transpiration maps throughout the dry season, it was therefore necessary to extrapolate temporally the available data. Several modelling techniques to simulate sap flow measurements have been reviewed, each with different levels of accuracy and complexity (Liu et al., 2009; O'Brien et al., 2004; Stöhr and Lösch, 2004; Verbeeck et al., 2007; Wheeler and Stroock, 2008; Whitley et al., 2009; Williams et al., 2001). We selected two modelling approaches that use typically measured climatic variables, namely: (1) a simple empirical micro-climatic model as described by Cienciala et al. (2000); and (2) artificial neural networks (ANNs) (Liu et al., 2009; Whitley et al., 2009). These two approaches were tested using customized scripts in MATLAB to choose the one that best simulated the available time-series data.

The empirical approach proposed by Cienciala et al. (2000) is based on combining the non- linear response of Q_s to short-wave radiation and air relative-humidity, using the following equation:

$$Q_s = \frac{aR_s}{[(c + R_s) \times (100 - b \times RH)]} \quad (2)$$

where a, b, c are fitted parameters, R_s is the short wave incoming solar radiation ($W\,m^{-2}$) and RH (%) is the air relative-humidity. The parameters a–c were first optimized to follow seven continuous days of Q_s measurements of *Q.i.* and seven days of *Q.p.* in each tree size-category. Afterwards, the model was used to calculate Q_s throughout the dry season to assess its accuracy as compared to the ANN.

The ANN is a purely statistically based response of Q_s to the meteorological forcing on a time-step basis (Abramowitz, 2005).

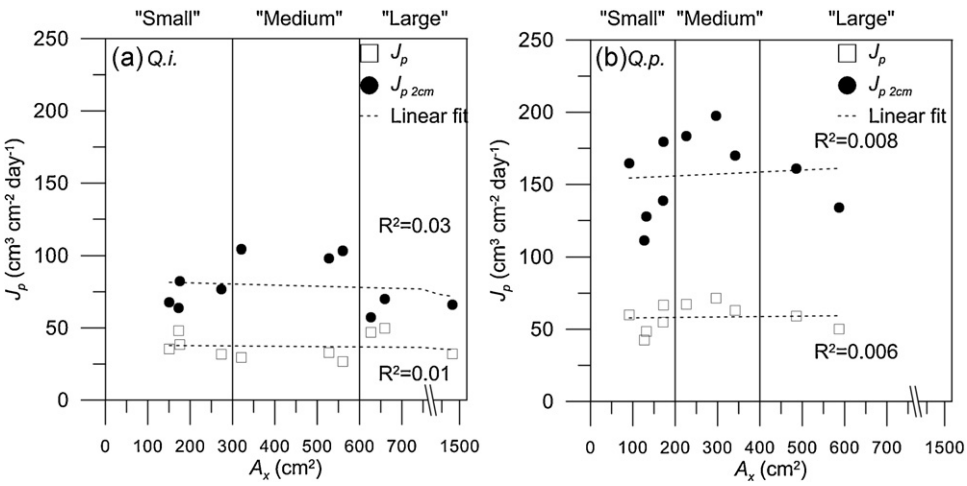

Fig. 2. Variability of two types of daily sap-flux density, the first averaged across whole xylem depths (0.5–7.5 cm) (J_p) and the second averaged across 2 cm xylem depth ($J_{p\,2\,cm}$). J_p and $J_{p\,2\,cm}$ are expressed as a function of the xylem area (A_x) for (a) *Q.i.* and (b) *Q.p.* trees.

The ANN was built and optimized as described by Liu et al. (2009), using seven non-continuous days of Q_s measurements for training of the network. In our study, the ANN model included a vapour pressure deficit (VPD) of 2 m height, VPD of 6 m height, R_s, *RH* and wind speed (W_s) of 10 m height as the input variables (all normalized); Q_s was the output variable. The soil moisture component was not used as it was the case in the study of Liu et al. (2009), because the Q_s did not respond to the soil moisture dynamics during the dry season. The shallow water-table and the significant length of the roots of *Q.i.* and *Q.p.* trees, likely tapping groundwater whenever demanded, explain the negligible response of Q_s to soil moisture variability. Therefore, it was safe to assume that the dry season tree-transpiration in the Sardón catchment was driven mainly by the variation in climatic conditions.

The structure of the ANN models for simulating Q_s in *Q.i.* and *Q.p.* consisted of three neural layers: an input layer, a hidden layer, and an output layer. The transfer functions used for the hidden and output layers are, hyperbolic–tangent–sigmoid transfer function (tan–sig) and logarithmic–sigmoid transfer function (log–sig), respectively, as described by Liu et al. (2009). After deriving *Q.i.* and *Q.p.* ANN models, they were used to calculate Q_s throughout the entire dry season.

For validating both modelling techniques, the Q_s outputs were compared to Q_s measurements from 6 additional dry-season days (fulfilling dry-season standard) using the assessment procedure described by Ritter et al. (2011). They proposed to use the Nash Sutcliffe Efficiency (*Ceff*) index (McCuen et al., 2006) in a goodness-of-fit evaluation protocol referred as FITEVAL. The FITEVAL procedure is programmed in MATLAB and combines the calculation of various error indices to evaluate the performance of the model versus real Q_s measurements, taking into consideration the effect of outliers and providing a probability density function to better discriminate the agreement between modelled and real Q_s. The final result is a probability distribution of the *Ceff* index typically between 0 and 1 (1 = best fit), ranked by four categories as follows: "very good" (*Ceff* = 0.9–1), "good" (*Ceff* = 0.8–0.899), "acceptable" (*Ceff* = 0.65–0.799) and "Unsatisfactory" (*Ceff* <0.650).

2.5. Remote sensing tree classification

In the Sardón catchment there are two different oak tree species, *Q.i.* and *Q.p.*, that had to be classified applying remote sensing technique. This was done by combining: (1) a supervised classification; (2) an object-oriented classification; and (3) a comparison of seasonal variation of the two tree species. The classification was applied on two satellite images of high spatial resolution (60–40 cm per pixel), acquired in two different seasons, namely: a QuickBird image during the 2009 (August) dry season and a WorldView-II image during the 2010 (December) wet season. Both satellite images were 4-bands multispectral, orthorectified, pan-sharpened and obtained with 0% cloud cover and a <10° nadir.

The first step of supervised classification using the 2009 QuickBird image of dry season did not yield sufficient accuracy. The second step of object-oriented classification improved the accuracy but still there was partial overlap of the electromagnetic spectra of *Q.p.* and *Q.i.* trees, in addition to their confusingly similar canopy shapes. Therefore, as *Q.i.* is an evergreen species and *Q.p.* is a deciduous species, an additional winter-season image was used to discriminate between leafless *Q.p.* and *Q.i.* The map obtained after the tree-species classification is referred below as the "classification map".

In the first step, the images were processed by a supervised classification using the ERDAS Imagine software to delineate the areas covered by tree canopies, as described by Ehlers et al. (2003). The supervised classification used the electromagnetic spectral values of the green, red and near infrared bands, which are sensitive to chlorophyll in vegetation (Janssen et al., 2001). The classification algorithms were trained by using the trees identified in the field survey (90 for *Q.i.* and 84 for *Q.p.*). The results of the supervised classification contained the tree canopy area coverage, but without distinction of species type at this stage.

In the second step of an object-oriented classification, spectral information and canopy shapes (object attributes) were used to discriminate between *Q.i.* or *Q.p.* species and to filter out other plants such as grasses and shrubs (Baatz et al., 2001; Dorren et al., 2003; Kimani et al., 2007). A multi-resolution segmentation algorithm and fine-tuning of the classification attributes (shape and compactness) was sufficient to define and delineate the tree canopies, thanks to the sharp contrast with the background (granitic soil in open woodland). The classified canopies were further smoothed using a morphology algorithm to reshape odd canopy shapes. To apply the classification algorithm, the image was divided into tiles of 1 ha area, batch processed with the classification algorithm and finally merged back into one single image using eCognition developer 8.7 (Trimble Germany GmbH). Dividing the image into tiles for batch-processing was necessary to reduce computing load and processing time. The object-oriented tree classification of the 2009 image, including both *Q.i.* and *Q.p.* species, resulted in an overall accuracy of 70%. This level of accuracy was considered insufficient for the transpiration scaling-up exercise, and thus the second image

during winter time (WorldView-II) was used to define the canopies of *Q.i.* only, as *Q.p.* had no leaves during this period. The object-oriented tree classification of the 2010 image was obtained using the same image processing as the 2009 image with overall accuracy of ~95%.

In the final step to achieve the highest possible classification accuracy, the results of the object-based classifications of the 2009 Quickbird dry-season image and of the 2010 WorldView-II wet-season image were cross-referenced using the spatial-selection tool of ArcMap 10 (ESRI, Inc.). In this way, the information about *Q.i.* in the 2010 map was transferred into the target classification map of the 2009. To execute the spatial-selection tool, the 2009 classification map was used as the "target" to assign the *Q.i.* trees present in the 2010 classification map, which was defined as the "source". The re-classification of misclassified *Q.i.* tree canopies was carried out directly in the "Attribute Table" of the map. Likewise, *Q.p.* canopies misclassified as *Q.i.*, and identified by their absence from the 2010 classification map, were re-assigned as well. The resulting vector layer was a tree-species classification map of *Q.i.* and *Q.p.* containing canopy areas classified per species for all the trees in the Sardón catchment. Such a classification map of Mediterranean *Quercus* sp. species can be considered as valid for several years because the change of the vegetation coverage in Mediterranean forests is naturally slow, a result of the dry inter-annual conditions that limit the growth rate (Corcuera et al., 2004; Hernández-Santana et al., 2009) and limited human intervention in the Sardón catchment (Lubczynski and Gurwin, 2005).

2.6. Accuracy assessment of the tree classification

To validate the tree-classification of *Q.i.* and *Q.p.*, an accuracy assessment was applied as described by Congalton (1991). This accuracy assessment is based on the elaboration of an error matrix and the calculation of four accuracy indexes: (1) overall accuracy, (2) user's accuracy, (3) producer's accuracy, and (4) the Kappa coefficient. This assessment procedure has been used extensively with diverse types of land cover thematic maps (Giles, 2002), and for tree-species classifications derived from remotely sensed data (Carreiras et al., 2006; Kimani et al., 2007).

To populate the error matrix, a large data set of ground-control points is needed (see Fig. 1). Dividing the area into sample plots (Stehman and Czaplewski, 1998) and elaborating error matrices with ground-control points of those plots (Hay, 1979) is a common practice for the evaluation of land-cover maps (Giles, 2002). We used a simple random sampling for the whole catchment (Stehman and Czaplewski, 1998), since conditions were quite uniform across the relatively small catchment (≈80 km^2). 800 tree ground control points (128 for *Q.i.* and 672 for *Q.p.*) were selected randomly from trees located in 4 macro-plots established for the biometric survey (Reyes-Acosta and Lubczynski, 2012). Additional to those 800 trees, 208 trees were used in the training of the classification algorithms for both species. The 800 ground-control points were compared with the classification map using the spatial-join tool, and evaluated with a Boolean expression to quantify the matching records as follows: if the ground-control points species was the same as in the map classification, then the expression was = 1, if false = 0. The results of this procedure were used to fill the error matrix by totalising the correctly classified and misclassified trees. Once the error matrix was filled (Table 2), the "overall accuracy", "user's accuracy", "producer's accuracy", and Kappa coefficient indexes were calculated using 800 ground-control points following the equations of Giles (2002) as bellow:

$$\text{overall accuracy} = \frac{\sum_{i=1}^{q} n_{ss}}{n} \times 100\% \tag{3}$$

where "overall accuracy" is a straightforward index of the overall accuracy in the analysed map layer, q is the number of species categories, s is a species-specific category index, $\sum_{i=1}^{q} n_{ss}$ is the sum of all correctly classified tree canopies, n is the total number of ground-control points used in the assessment.

$$\text{user's accuracy} = \frac{n_{ss}}{n_{s+}} \tag{4}$$

where "user's accuracy" is a measure of commission error of the classified categories indicative of the probability that a classified canopy actually represents that species category on the ground (Story and Congalton, 1986); s is a species-specific category index, n_{ss} is the total number of correctly classified canopies in a species category; and n_{s+} is the total number of classified canopies that were classified in that species-specific category (Congalton, 1991; Giles, 2002).

$$\text{producer's accuracy} = \frac{n_{ss}}{n_{+s}} \tag{5}$$

where "producer's accuracy" is a measure of omission error of the classified categories, indicating the probability of a ground point to be correctly classified in a species-specific category (s); n_{ss} is the total number of correctly classified canopies in a species category; and n_{+s} is the total number of ground-recognised canopies that were classified in that species-specific category (Congalton, 1991; Giles, 2002).

Additionally, the Kappa Index of Agreement (KIA) was calculated to account for the possibility of correctly classifying the tree canopies by random guessing (Cohen, 1960; Congalton, 1991; Giles, 2002; Kimani et al., 2007). This is particularly relevant for the obtained tree classification in this study because in the Sardón catchment there are two tree species and one of them (*Q.p.*) is more common than the other (see Section 3.5), hence there is an inherited probability of properly classifying the tree canopies if all canopies were to be classified as the dominant one. The KIA is calculated as follows:

$$KIA = \frac{n \times \sum_{i=1}^{q} n_{ss} - \sum_{i=1}^{q} (n_{s+} \times n_{+s})}{n^2 - \sum_{i=1}^{q} (n_{s+} \times n_{+s})} \tag{6}$$

where, q is the number of species-specific categories; s is a species-specific category index; n_{ss} is the number of correctly classified canopies in a species category; n_{s+} and n_{+s} are the marginal totals of correctly classified canopies and ground-recognized canopies respectively, for each species-specific category; and n is the total number of observations (Congalton and Green, 1999). When the obtained agreement is within the probability of a random classification the KIA value is zero, while 1 indicates 100% of agreement (Cohen, 1960). KIA values >0.80 (80%) indicate strong agreement, between 0.40 and 0.8 (40–80%) moderate agreement and <0.40 (40%) poor agreement (Congalton, 1996).

2.7. Scaling up sap flow measurements for transpiration mapping

In this study, the individual tree sap flow measurements (Q_s) were considered to be equal to the amount of water transpired by a tree (Wullschleger et al., 1998; Lubczynski, 2009). Based on that assumption, Q_s measurements were scaled up as described by Lubczynski (2009) using the following four elements: (1) a parameter to be scaled-up, (2) a scalar used for scaling-up, (3) a "Biometric Upscaling Function" (BUF), and (4) a scaling-up technique.

A scaling-up parameter (e.g. sapwood area (A_x) or sap flow (Q_s)) is a parameter that is directly needed for quantifying transpiration but is difficult to define spatially. Its spatial variation can be defined (scaled up) by an easily measurable scaling-up scalar extrapolated using a BUF and an appropriate scaling-up technique. In this study

we decided to use A_x as the scaled-up parameter because, in contrast to Q_s, A_x is nearly temporally independent so its scaling up is more reliable.

The selection of scalar depends on the scale of the transpiration assessment. In general, two different spatial scales of transpiration mapping can be considered: (i) plot or stand scale transpiration (T_{sta}); and (ii) catchment transpiration (T_c). For T_{sta}, stem areas (A_s) are typically used as scaling-up scalars, because A_s is known to be well-correlated with A_x (Kumagai et al., 2005; Čermák et al., 2004) and can be measured from single trees at the plot or stand scale. At the catchment scale, such as the whole Sardón catchment (≈80 km^2), it would not be practical and feasible to measure each single tree for A_s. Therefore, we used the canopy areas (A_c) as the scalar instead, as the A_c is retrievable from the high resolution images.

The third element necessary for scaling up sap flow measurements are the "Biometric Upscaling Functions" (BUFs). The BUFs are field-defined, paired, species-specific relations between scalars and scaled parameters (Lubczynski, 2009). To properly select the BUFs for *Q.i.* and *Q.p.*, pairs of selected scalars (*DBH*, A_s and A_c) and scaled parameters (A_x) were evaluated with a Pearson product-moment correlation-coefficient (r) matrix (Quinn and Keough, 2002) and then regressions were calculated and described by the coefficient of determination (R^2). These coefficients evaluate the potential of the parameters (in this case a scaling-up scalar) to predict the others (in this case scaling-up parameters) using the proposed regressions (Quinn and Keough, 2002). The result of the analysis was used to determine the highest R^2 from the selected pairs of parameters (i.e. *DBH* vs. A_x and A_c vs. A_x), thus highlighting the best linear or polynomial models from the pairs of parameters to be used as BUFs. To properly cover the natural variability of the scalars and scaled-up parameters 90 *Q.i.* and 84 *Q.p.* tree samples were used to derive the BUFs. This sample size guaranteed that the natural variability of the biometric characteristics was properly accounted for as discussed in Reyes-Acosta and Lubczynski (2012).

The fourth element necessary for the scaling-up process was the scaling-up technique. For this study, we selected remote sensing as the scaling up technique because: (1) the size of the Sardón catchment (≈80 km^2) did not permit an in situ assessment of tree transpiration; (2) the remote-sensing technique allowed for an automated classification of the tree species and an efficient measurement of the canopy areas for the whole catchment (the scalar in this study); (3) the Sardón catchment is covered by open woodland, which facilitates an accurate definition of individual tree canopies, when using high-resolution remotely-sensed images; (4) tree-species classification was relatively simple due to the two-species composition (one deciduous, one evergreen) of the vegetation in the study area, which resulted in a highly accurate classification; and finally (5) the high R^2 for the BUFs indicated a good prediction potential.

The methodology of transpiration mapping at the catchment scale (T_c) followed the series of steps depicted in Fig. 3. First, after classifying the tree canopies per species, the projected areas of the canopies (A_c) were automatically calculated using GIS tools from the classification map. For those cases in which several trees were naturally arranged in one cluster, they were considered as a single larger tree with biometric characteristics equal to the sum of the biometric parameters of the individual trees. Second, species-specific BUFs were established. Third, using the BUFs of *Q.i.* and *Q.p.*, the scaled up A_x was calculated for all the trees in the entire catchment. Fourth, using geometric equations, the A_x areas of all the trees were divided into annuli areas (ring-like) representing concentric sapwood areas (A_{xi}) of 1 cm thickness (Fig. 3). This was done to take into consideration the radial variability of the sap flux density (J_{pi}) obtained by optimised J_{pi} measurements as presented by Reyes-Acosta and Lubczynski (2012). Fifth, Q_s of individual trees was calculated as a sum of Q_{si}^{sc} of each individual annulus per tree-size category, as follows:

$$Q_s = \sum_{i=1}^{n} Q_{si}^{sc} = \sum_{i=1}^{n} [A_{xi} \times J_{pi}^{sc}]\,[\mathrm{l\,day^{-1}}] \tag{7}$$

where each Q_{si}^{sc} is defined as a product of sapwood area (A_{xi}) and ith sap-flux density (J_{pi}^{sc}) of the corresponding sapwood annulus for each tree-size category (sc). The subscript n is the total number of annuli. In the case of trees with a sapwood depth > 7.5 cm (max depth of HFD), it was assumed that the rest of the sapwood transported a linearly decreasing with depth amount of sap flow until it became zero in the heartwood. Sixth, to obtain the canopy-normalised sap flow, also referred as canopy transpiration (T_t), each Q_s was divided by the area of its own canopy to obtain T_{t-Qi} and T_{t-Qp} as follows:

$$T_t = \frac{Q_s}{A_c} = J_p \times \frac{A_x}{A_c} \quad [\mathrm{mm\,day^{-1}}] \tag{8}$$

Seventh, to calculate the transpiration of a stand, the sum of all tree water-uptakes in a stand ($\sum_{j=1}^{n} Q_{sj}$) was divided by the corresponding stand area (A_{sta}), as in Eq. (9). The sub-index j refers to each single tree in the stand and m to the number of trees in the stand.

$$T_{sta} = \frac{\sum_{j=1}^{m} Q_{sj}}{A_{sta}} \quad [\mathrm{mm\,day^{-1}}] \tag{9}$$

For this study, we have chosen an area of 1 ha for the analysis of the stands, thus the catchment area was discretised using a 1 ha grid. To calculate T_{sta} for each grid in the catchment, the tree-classification map was first segmented by the grid using the spatial-join tool of ArcMap 10. Then the Q_{sj} of each segmented canopy was summed for each cell in the grid and divided by the area of a single cell of the grid (A_{sta} = 1 ha) to calculate T_{sta}. For the relative-contribution of canopies that crossed cell boundaries, a canopy fractions approach was applied to calculate T_{sta}. An example of three different cases of cells' boundaries overlap can be seen in Fig. 3, namely: (1) the contribution of single canopy segments (A_{c1}^{c} and A_{c1}^{d}), each one in a different cell (defined as T_{sta1} and T_{sta2}, respectively); (2) the contribution of two canopy segments (A_{c2}^{b} and A_{c1}^{b}) from two separate trees in one cell (defined as T_{sta3}); and (3) the contribution of a full canopy (A_{c4}) together with canopy segments of two separate trees (A_{c2}^{a} and A_{c1}^{a}) inside one cell (defined as T_{sta4}). For each case, Eq. (9) was transformed to fit the arrangement of the segments in each cell, thus obtaining Eqs. (10)–(12). For T_{sta1} and T_{sta2}, Eq. (10) was used, for T_{sta3}, Eq. (11) was used, and for T_{sta4} Eq. (12) was used. A_{c1}, A_{c2}, and A_{c3} define the entire canopy area of each tree.

$$T_{sta1} = \frac{Q_{s1}(A_{c1}^{c}/A_{c1})}{A_{sta}} \quad \text{and} \quad T_{sta2} = \frac{Q_{s1}(A_{c1}^{d}/A_{c1})}{A_{sta}} \tag{10}$$

$$T_{sta3} = \frac{Q_{s2}(A_{c2}^{b}/A_{c2})}{A_{sta}} + \frac{Q_{s1}(A_{c1}^{b}/A_{c1})}{A_{sta}} \tag{11}$$

$$T_{sta4} = \frac{Q_{s1}(A_{c1}^{a}/A_{c1})}{A_{sta}} + \frac{Q_{s2}(A_{c2}^{a}/A_{c2})}{A_{sta}} + \frac{Q_{s3}(A_{c3}/A_{c3})}{A_{sta}} \tag{12}$$

After processing all cells in the map using Eqs. (10)–(12), and also variations of these for stands holding >3 canopy segments, the resultant map contained hectare-specific values of transpiration in 1 ha quadratic grid expressed in mm day^{-1} (T_{sta}). To calculate transpiration at the catchment level as a total (T_c), an average T_{sta} of all grid cells was calculated.

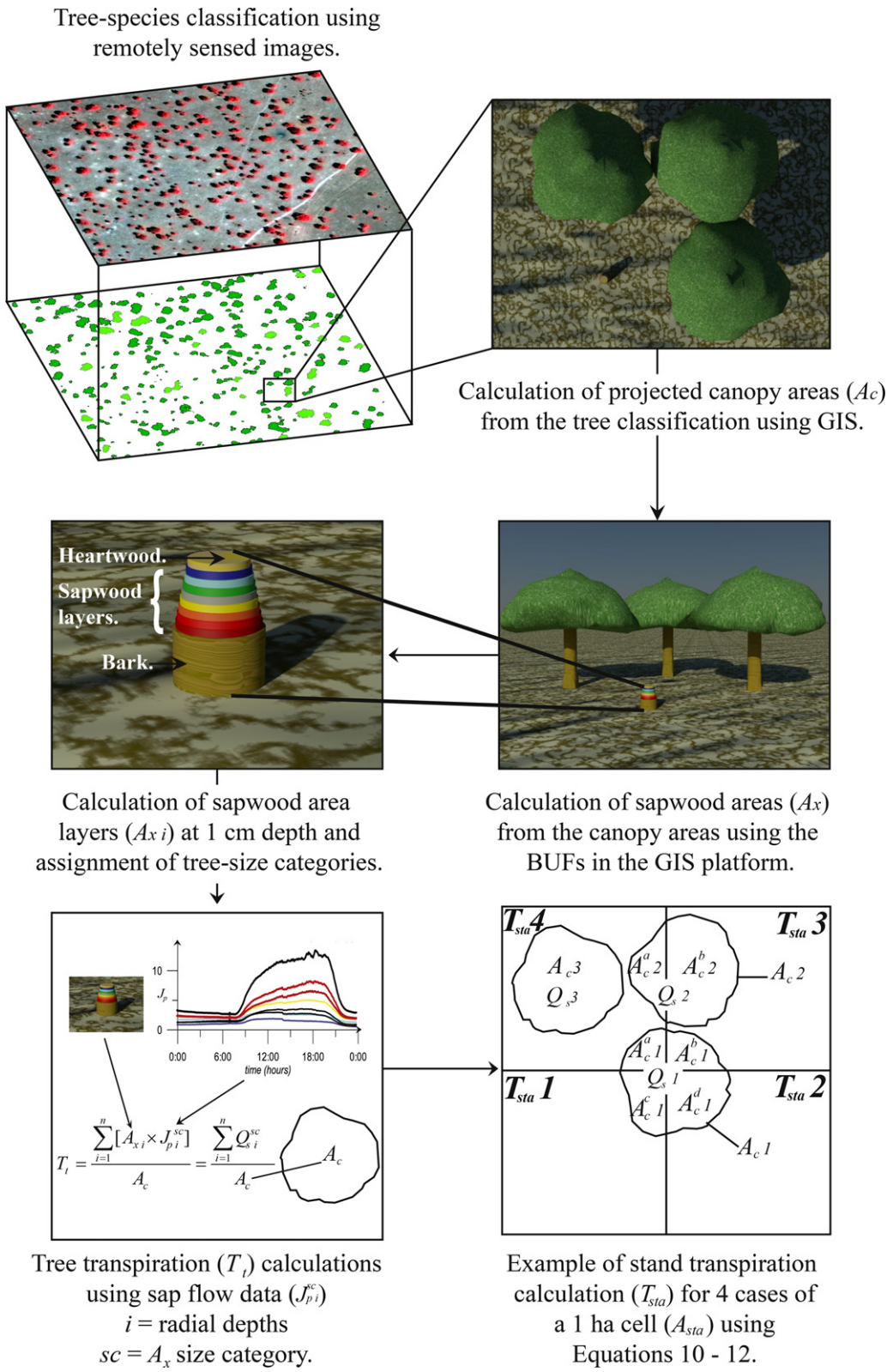

Fig. 3. Summary of the main steps of tree transpiration mapping at catchment scale.

2.8. Assessment of remote sensing scaling-up procedure

In order to evaluate the performance of scaling up using remote sensing, we compared it to in situ stand-scale (i.e. plot) scaling up followed by an uncertainty analysis. For that purpose, we selected a 1 ha stand (100 m × 100 m) in which all trees in that stand (7 *Q.i.* and 6 *Q.p.*) were measured and the scaling-up procedure performed using a BUF relating *DBH* with A_X. For the remote-sensing scaling up of the same plot, the BUF relating A_c (as obtained by the attributes of the classified canopies) with A_X was used.

For the uncertainty analysis we applied a Monte-Carlo simulation using the probability distributions of the error associated with

two of the most important steps of the remote sensing scaling up, namely: (1) the uncertainty from misclassified classes (*Q.i.* or *Q.p.*, respectively) in the tree classification map, and (2) the uncertainty in the confidence interval of the derived BUFs.

Additional factors such as installation errors, equipment malfunctioning limitations, natural variations in the sapwood tissue, etc. also influence the accuracy of sap flow measurements. However, to account for all those factors is very complex, which was outside the scope of this research. Nevertheless, the optimisation technique used to acquire the sap flow measurements was designed to enhance the accuracy and obtain the highest accuracy possible (Reyes-Acosta and Lubczynski, 2012).

To properly define the error for the species classification we used a random binomial distribution defined by the probability calculated in the "user" accuracy assessment. Using a binomial distribution is justified because the error probability for the classification maps is limited to just two species. To account for the error of the BUFs, we used a random normal distribution derived from a 99% confidence interval, because the distribution of the norm of residuals of a least-squares linear fit is assumed to follow a normal distribution (Rice, 2006).

The Monte-Carlo simulations were run for 1000 iterations to reach a satisfactory convergence of the tree transpiration calculations. For each iteration, the random binomial distribution was first simulated and then followed by the random normal distribution simulation. At the end of each iteration, T_c was calculated according to the equations given in the Section 2.7, using as input the random species classification and the species-specific random A_x values of each BUF (for *Q.i.* and *Q.p.*). After 1000 iterations, the distributions of the outputs were examined.

3. Results and discussion

3.1. Tree biometric characteristics

The frequency histograms of the biometric characteristics of 90 *Q.i.* trees and 84 *Q.p.* trees (diagonals in Fig. 4) followed a quasi-normal distribution skewed to the left. The distribution of the biometric parameters indicated that the tree population for both species was mostly composed of small – to medium – tree-stem sizes (*DBH* <0.5 m and A_s <0.25 m^2), with small – to medium canopy areas (A_c <50 m^2) (Table 3) and small xylem areas (A_x <0.05 m^2). The trees with small- to medium-size *DBH*, held more than 90% of the total sapwood tissue for both tree populations. Big trees with large canopies (>100 m^2) and big trunk sizes (>0.70 m) were rare and distinct but due to their scarcity they were less significant as contributors to the catchment's tree transpiration.

3.2. Sap flow measurements

3.2.1. Categorization of the A_x vs. J_p dependence

J_p measurements used in this study are described in Reyes-Acosta and Lubczynski (2012). For the proposed scaling up procedure, the relation between A_x and J_p is critical. Linearity tests of average $J_{p\,i}$ at 0.5 cm and 1.5 cm depths in the sapwood ($J_{p\,2\,\mathrm{cm}}$) and average $J_{p\,i}$ for all sapwood annuli (J_p), from 10 *Q.i.* and 10 *Q.p.* trees, indicated a very low correlation with A_x for *Q.i.* (R^2 = 0.03 for $J_{p\,2\,\mathrm{cm}}$ and R^2 = 0.01 for J_p) and *Q.p.* (R^2 = 0.008 for $J_{p\,2\,\mathrm{cm}}$ and R^2 = 0.006 for J_p), indicating no significant dependence between A_x and J_p. Instead, as seen in Fig. 2 for *Q.i.* and *Q.p.*, $J_{p\,2\,\mathrm{cm}}$ depicted an increment towards the "medium" A_x values and then decreased again towards the "large" A_x values (Fig. 2). Such pattern was not present in the relation of J_p (average sap-flux density across the sapwood profile) with A_x. The described $J_{p\,2cm}$-A_x pattern implied that the largest $J_{p\,2\,\mathrm{cm}}$ occurred in the trees of the medium size.

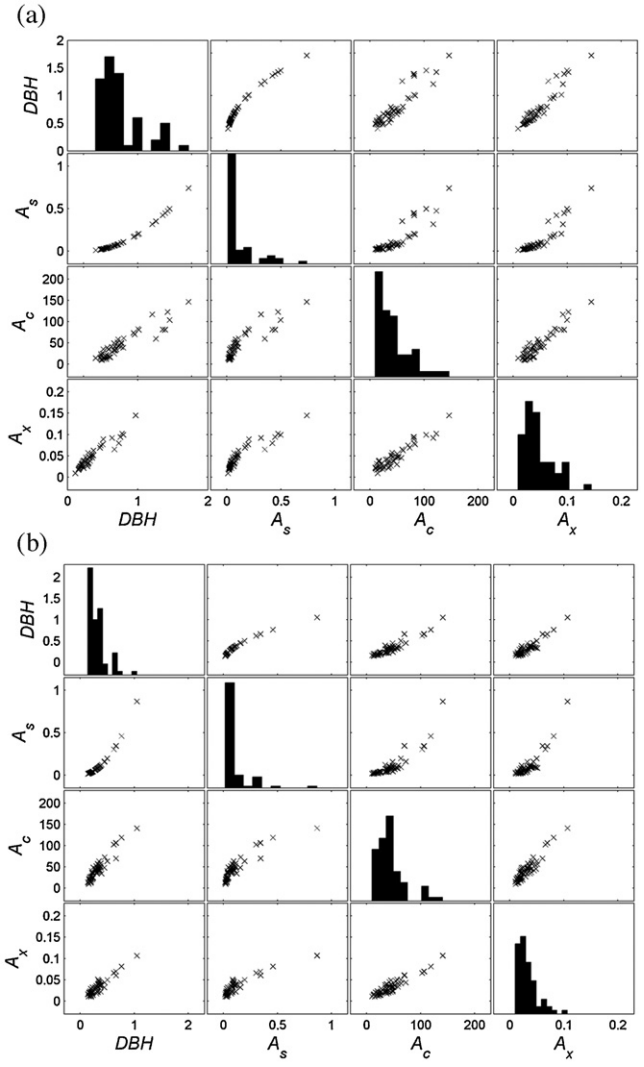

Fig. 4. Cross-correlation matrix of the biometric parameters measured in the survey for (a) *Q.i.* and (b) *Q.p.* trees. Diameter at breast height (*DBH*) is in m, area of the stem (A_s) is in m^2, ground-projected canopy area (A_c) is in m^2, and xylem area (A_x) is in m^2.

Considering that the outermost 2 cm of the *Q.i.* and *Q.p.* sapwood typically conducted most of Q_s (Reyes-Acosta and Lubczynski, 2012), not only due to the largest J_p, but also due to the largest corresponding annuli sapwood areas (external sapwood rings are the largest), and that the $J_{p\,2\,\mathrm{cm}}$ significantly varied with A_x, a categorization of the sap flux density measurements as dependent on A_x was necessary. Even though the differences between $J_{p\,2\,\mathrm{cm}}$ as presented in Fig. 2 were low, they were significant because of the multiplicative effect of the outermost sapwood layer, implying that small differences of $J_{p\,2\,\mathrm{cm}}$, resulted in large differences of Q_s.

It is important to clarify that boundaries for the size-categories were intentionally set at different thresholds for both species, *Q.i.* and *Q.p.*, in order to better reflect the variability of the sap-flux density as dependent on the tree population structures. As a result, the derived A_x categories of sap flux density (Fig. 2) also listed in Table 1, have species-specific A_x ranges, except for the category "large" with common threshold ≥400 cm^2. Considering $J_{p\,2\,\mathrm{cm}}$ as reference for categorization, the highest average values in both species belonged to the "medium" category and were 101.9 cm^3 cm^{-2} day^{-1} for *Q.i.* and 179.3 cm^3 cm^{-2} day^{-1} for *Q.p.* trees. For the categories "small" and "large", the $J_{p\,2\,\mathrm{cm}}$ was significantly lower (Table 1).

Table 1
J_p and $J_{p\,2\,cm}$ in the tree-size categories of *Q.i.* and *Q.p.* A_x in cm^2 and J_p and $J_{p\,2\,cm}$ in $cm^3\ cm^{-2}\ day^{-1}$.

A_x tree-size category	J_p for *Q.i.*	$J_{p\,2\,cm}$ for *Q.i.*	J_p for *Q.p.*	$J_{p\,2\,cm}$ for *Q.p.*
Small				
<300 *Q.i.*	38.36	72.67	54.66	145.11
	(7.01[a])	(9.72[a])	(9.64[a])	(28.87[a])
< 200 *Q.p.*				
Medium				
300 ≤ *Q.i.* < 400	29.71	101.92	65.85	179.27
	(3.11[a])	(3.34[a])	(6.23[a])	(18.23[a])
200 ≤ *Q.p.* < 400				
Large				
	42.91	64.47	56.61	152.03
≥ 400	(9.53[a])	(6.43[a])	(9.06[a])	(25.44[a])

[a] Standard deviations.

It seems that such $A_x - J_{p\,2\,cm}$ distribution is not uncommon. For example Chavarro et al. (2009) in savannah trees of the Kalahari and Köstner et al. (1998) in a Scots pine plantation also found that the largest $J_{p\,2\,cm}$ was attributed to medium size trees $A_x - J_{p\,2\,cm}$ distribution. The presented $J_{p\,2\,cm}$ categorization substantially improves the accuracy of scaling of sap flow measurements. After confirming variable A_x–$J_{p\,2\,cm}$ distribution (for example with HFD) that can be categorised, we recommend to use the categorisation of $J_{p\,2\,cm}$ as proposed in this study.

The results from the sap flow field measurements showed that both $J_{p\,2\,cm}$ and J_p were higher in *Q.p.* than in *Q.i.* trees for all categories (Table 1), while *Q.i.* trees tended to be more active in deeper sapwood layers (5–7 cm deep) than *Q.p.* trees (active until 4 cm deep) (Reyes-Acosta and Lubczynski, 2012). These results imply that individual *Q.p.* trees of the same A_x as *Q.i.* contributed more to the water uptake. An interesting observation was made that the *Q.i.* and *Q.p.* species had relatively low variability of J_p around their means (Fig. 2), confirmed by low standard deviation (Table 1). This low variability suggests that growing *Q.i.* and *Q.p.* trees increase their water uptake (Q_s) proportionally to A_x so also to A_s that increases with tree growth.

3.2.2. Temporal extrapolation of sap flow measurements

The dry-season temporal extrapolation using the "Cienciala Model" (CM) and artificial neural networks (ANNs) was carried out in 3 months period of 2009 (from 15 June to 15 September), to assess the dry-season temporal variability of sap flow and tree transpiration in that period.

Evaluation of the performance of the CM and ANN showed that the goodness-of-fit of the Q_s simulations using the ANN method was "very good" for *Q.i.* (*Ceff* between 0.92 and 0.96) and *Q.p.* (*Ceff* between 0.97 and 0.99) (Fig. 5). Significantly lower accuracy was obtained by applying CM. For *Q.i.* the *Ceff* was between 0.75 and 0.85, indicating a goodness-of-fit between "acceptable" and "good", while for *Q.p.* the *Ceff* was between −0.60 and −0.11, indicating an "unsatisfactory" goodness-of-fit (Fig. 5). This was mainly because the night flow of *Q.p.* trees was not taken in consideration by the CM model. The better performance of ANN as compared to CM was related to the use of more climatic drivers as inputs and the greater flexibility of the model. For the ANN method we used the vapour-pressure deficit at two heights ($VPD_{2\,m}$ and $VPD_{6\,m}$) and wind speed (W_s) at 10 m height, while in CM only incoming solar radiation and relative humidity at 2 m height were used. The additional climatic drivers used for the ANN are closely linked to the transpiration dynamics (Chu et al., 2009; Zeppel et al., 2004) and constrained the ANN sap flow calculations. Consequently, this is why the ANN approach was selected to simulate dry-season sap flow dynamics for both *Q.i.* and *Q.p.* species (Fig. 6a).

Table 2
Error matrix of 800 randomly selected ground-control points (canopies) used for the calculation of the error indexes of the tree-species classification map.

		Ground points		Total	
		Q.i.	*Q.p.*		
Mapped canopies	*Q.i.*	123 $n_{Q.i.-Q.i.}$	5 $n_{Q.p.-Q.i.}$	128	$n_{Q.i.+}$
	Q.p.	57 $n_{Q.p.-Q.i.}$	615 $n_{Q.p.-Q.p.}$	672	$n_{Q.p.+}$
Total		180	620	800	
		$n_{Q.i.+}$	$n_{Q.p.+}$		

The daily means and maxima Q_s obtained from the ANN-simulations showed a low temporal variability for both *Q.i.* and *Q.p.* trees (Fig. 6a). This was indicated by the low standard deviation (SD) between daily Q_s means (for *Q.i.* the mean of daily means was 825 $cm^3\ h^{-1}$ with SD = 151 $cm^3\ h^{-1}$ and for *Q.p.* 1611 $cm^3\ h^{-1}$ with SD = 151 $cm^3\ h^{-1}$). The overall good match between the modelled and measured transpiration, including good agreement with respect to the low temporal variability of daily Q_s means and maxima (Reyes-Acosta and Lubczynski, 2012), imply that the dry-season transpiration values scaled up from the dry-season standardised J_p data can be assumed to be representative for most of days during the dry season (July to September), i.e. for those days fulfilling the criteria of the "standard" dry-season day (see Section 2.3 for details on J_p standardisation).

The only considerable differences in Q_s temporal variability were noticed in some few days during dry season when some clouds and rain were present (Fig. 6a and b). These days were indicated by a considerably higher SD of Q_s (e.g. 400 $cm^3\ h^{-1}$ for *Q.i.* and 300 $cm^3\ h^{-1}$ for *Q.p.*). For such days the simulated Q_s was lower than measured. However these episodes were rare during the dry season, thus the scaling up estimations from standardized non-cloudy measurements represent the dominant dry-season transpiration in the Sardón catchment. In case of missing records in time series of sap flow measurements, the ANN modelling framework can be used to simulate the missing measurements and consequently calculate catchment transpiration in any conditions, assuming that the ANN framework can reflect the effect of cloudy–rainy conditions in the sap flow. Unfortunately, in this study was not possible to validate this assumption because there was no opportunity to monitor sap flow on those very few cloudy–rainy days in dry season.

3.3. Accuracy of the tree classification

Accurate tree classification is an important component of the sap-flow scaling-up method, particularly when trees of different species but the same A_c have significantly different Q_s. This was the case in our study, because both tree species, *Q.i.* and *Q.p.*, differed in dry-season sap flow.

The "Overall accuracy" (Eq. (3)) of the tree classification map was 90%, which is the probability that any randomly chosen tree canopy in the classification map was correctly assigned. Regarding the other accuracy indexes (as calculated by using the error matrix of misclassified trees in Table 2), it was found that the "User's accuracy" (Eq. (4)) for a randomly chosen *Q.i.* canopy in the map

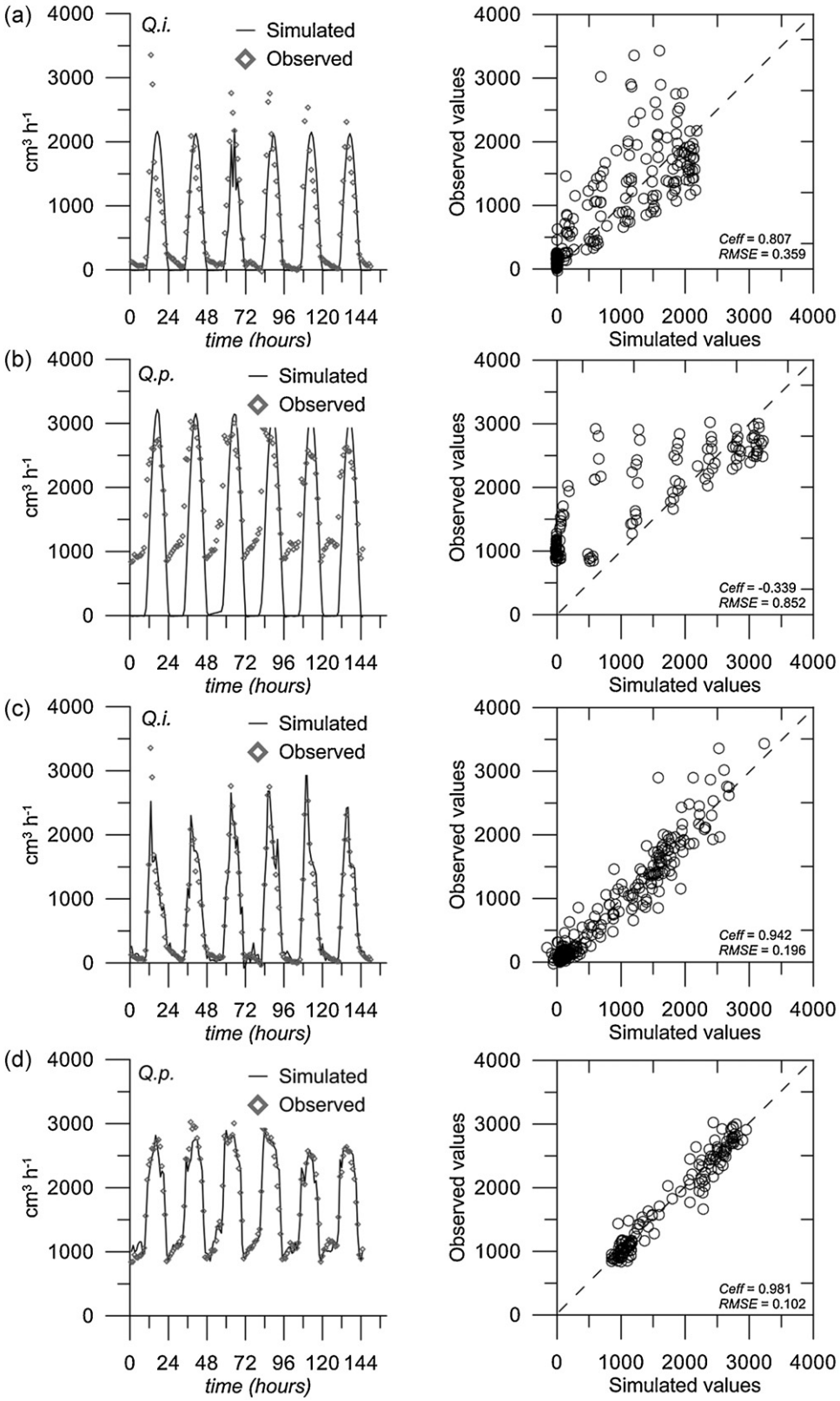

Fig. 5. FITEVAL assessment of the sap-flow simulation results for (a) Cienciala model, *Q.i.*; (b) Cienciala model, *Q.p.*; (c) ANN model, *Q.i.*; and (d) ANN model, *Q.p.*

had a higher probability (96%) of being properly classified than the *Q.p.* canopy (92%). Conversely, "Producer's accuracy" (Eq. (5)) indicated that a *Q.p.* canopy randomly chosen in the field had a higher probability (90%) of being properly classified than a *Q.i.* canopy (68%). These indexes indicated that the accuracy of the classification map for each species was sufficient and that it was dependent on the number of trees of each species. The average, catchment scale tree density for *Q.p.* was higher (19 trees ha^{-1}) than for *Q.i.* (4 trees ha^{-1}), thus increasing the probability of matching *Q.p.* ground control points with the classification map, but also

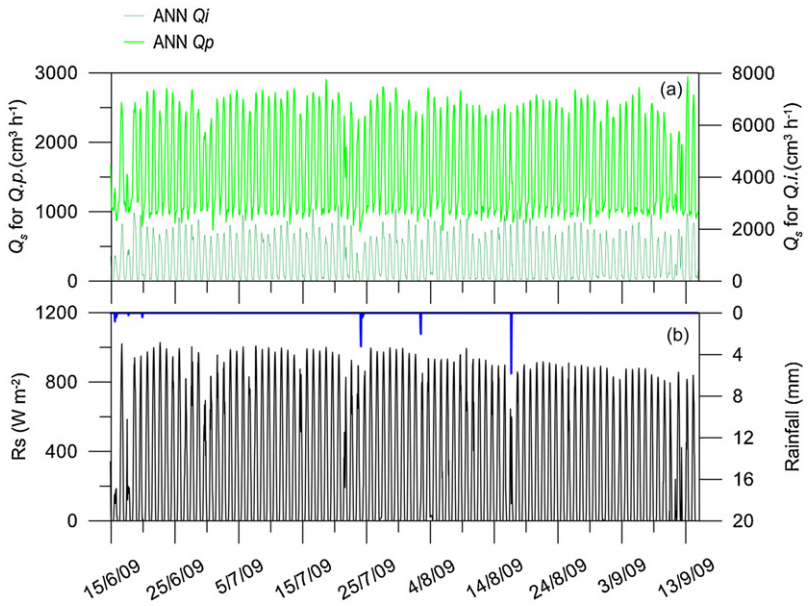

Fig. 6. Dry season temporal sap flow versus climatic temporal variability: (a) daily ANN sap-flow simulations during the dry season of 2009 (15 June–15 September) for *Q.i.* and *Q.p.* trees; (b) incoming solar radiation (*Rs*) and rainfall.

reducing the probability of successfully classifying all the *Q.i.* trees in the field.

The final accuracy index, the KIA (Eq. (6)), was 0.8. According to the qualitative scale for KIA values proposed by Congalton (1996), the obtained KIA value indicated strong agreement between the ground control points and the classification map, with a low probability of correctly classifying tree canopies by random guess alone. This further supported the validity of the classification map and its robustness for the scaling-up process.

Despite the difference found between the accuracies for each species, the accuracy assessment indexes indicated that the tree classification map was accurate, thus any misclassification of canopies in the map would have a minimal effect on the scaled-up transpiration calculations. This effect of misclassification is analysed and discussed further in Section 3.7.

3.4. Scalars, scaling-up parameters and BUFs

A preliminary assessment of the biometric characteristics using the Pearson product-moment correlation-coefficient matrix (r) showed a significant interdependence for various combinations of characteristics of both species (Fig. 4 and Table 4). *DBH*, A_s, A_c and A_x gave high r values for both species, indicating a strong interdependency and good potential for building a robust and precise BUF.

To establish the BUFs for *Q.i.* and *Q.p.* trees, A_x was selected as the scaled-up parameter because of its low temporal variability. A_c was selected as a remote-sensing-based scalar because it can be accurately defined on remotely sensed images of very high spatial resolution, and, finally, *DBH* as the stand scaling-up scalar because it is easy to measure in the field. The *DBH*-A_x of both species fitted a second grade polynomial equation, which resulted in $R^2 = 0.88$ for *Q.i.* trees (Fig. 7a) and $R^2 = 0.91$ for *Q.p.* trees (Fig. 7c). The A_c-A_x BUFs of both species fitted a linear equation, with the coefficients of determination $R^2 = 0.84$ for *Q.i.* trees (Fig. 7b) and $R^2 = 0.86$ for *Q.p.* trees (Fig. 7d). It is remarkable that although the differences between the BUFs of *Q.i.* and *Q.p.* were not large (Fig. 7), both BUF types (i.e. DBH-A_x and A_c-A_x) of *Q.i.* were steeperthan the ones of *Q.p.* This means that the BUFs of *Q.i.* had a larger A_x/A_c ratio than the BUFs of *Q.p.* indicating faster increase of A_x with the increase of *DBH* and A_c. Therefore, a canopy area recognized by remote sensing as *Q.i.* would have larger A_x than the same size canopy area of *Q.p.*

Table 4
Pearson product-moment correlation coefficient (r) matrix for the surveyed biometric parameters in *Q.i.* (90 trees) and *Q.p.* (84 trees).

	DBH	A_s	A_c	A_x
Q.i. trees				
DBH	1	0.98	0.87	0.86
A_s	0.98	1	0.84	0.83
A_c	0.87	0.84	1	0.86
A_x	0.86	0.83	0.86	1
Q.p. trees				
DBH	1	0.97	0.95	0.97
A_s	0.97	1	0.89	0.93
A_c	0.95	0.89	1	0.95
A_x	0.97	0.93	0.95	1

Table 3
Main statistics of the biometric parameters obtained in the survey for *Q.i.* ($n = 90$) and *Q.p.* ($n = 84$).

	DBH (m)		A_s (m²)		A_c (m²)		A_x (m²)	
	Q.i.	*Q.p.*	*Q.i.*	*Q.p.*	*Q.i.*	*Q.p.*	*Q.i.*	*Q.p.*
Min	0.11	0.14	0.01	0.02	9.88	10.02	0.01	0.01
Max	0.97	1.05	0.74	0.87	146.3	141.0	0.14	0.11
Mean	0.34	0.32	0.12	0.10	43.46	43.67	0.05	0.03
SD	0.20	0.17	0.15	0.13	30.73	25.66	0.03	0.02
Median	0.28	0.28	0.06	0.06	35.26	38.88	0.04	0.03

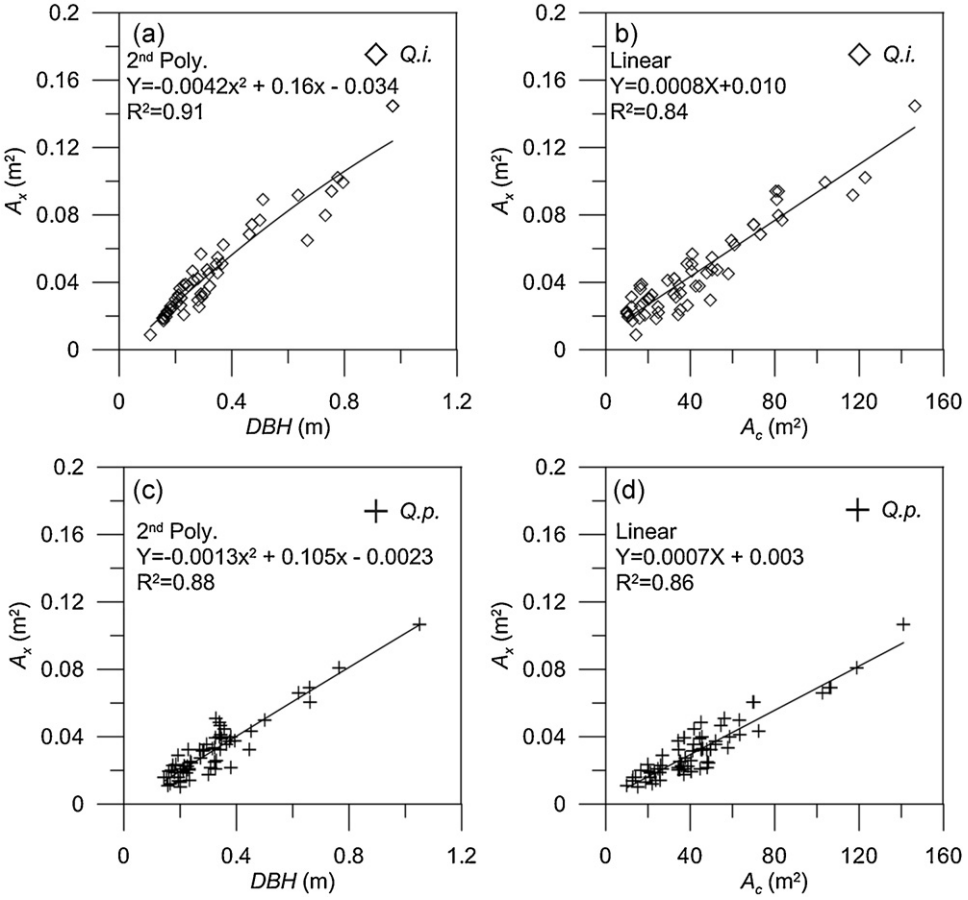

Fig. 7. Biometric scaling-up functions (BUFs) for *Q.i.* ($n = 90$) and *Q.p.* ($n = 84$) trees derived from the biometric measurements collected during the field survey. The BUFs (a) and (c) used for stand scaling-up follow a 2nd polynomial linear model for both species. The BUFs (b) and (d) used for remote-sensing-based scaling up follow a linear model. R^2 coefficient of determination.

The R^2 coefficients showed that using *DBH* as the scalar, yielded the best fits for both species, although using A_c as the scalar also provided high R^2, indicating a reliable BUF. The performance of both scaling-up techniques are compared and discussed in Section 3.6. Lubczynski and Gurwin (2005) also used A_c as a scalar and A_x as a scaling-up parameter in the same Sardón-catchment study area, but they obtained a much lower R^2 for both species (0.62), and their linear equations showed a higher proportion of A_x per unit of A_c (0.0022 for *Q.i.* trees and 0.0026 for *Q.p.* trees), than ours (0.0008 for *Q.i.* trees and 0.0007 for *Q.p.* trees). This discrepancy is likely to be related to the sample size, because Lubczynski and Gurwin (2005) sampled 22 *Q.i.* and 25 *Q.p.* trees, whereas we sampled 90 *Q.i.* and 84 *Q.p.* trees. Moreover, Reyes-Acosta and Lubczynski (2012) have demonstrated that the *DBH* size variability for *Q.i.* and *Q.p.* trees stabilizes after random sampling of more than 60 trees. A larger sample size gives better estimates of the characteristics of *Q.i.* and *Q.p.* tree populations, particularly for the characteristics of big trees (*DBH* >0.5 m), which greatly influence the BUFs' linear relations (Fig. 7). For future scaling-up studies on other species in open woodlands, we advise using a sampling design that effectively covers the natural variability of the trees (in our case >60 trees), such as stratified sampling (Reyes-Acosta and Lubczynski, 2012) or quartiles of the total (Čermák et al., 2004).

The analysis in this study confirmed the potential of using A_c as scalar for the remote sensing scaling up of sap flow measurements in large, sparse vegetation areas of WLE such as Sardón catchment. In contrast, *DBH* and A_s are rather to be used for scaling up at stand scale, because they cannot be retrieved from remotely sensed images.

3.5. Scaled up transpiration and spatial patterns

The scaled-up, canopy-normalised transpiration in the Sardón catchment for *Q.i.* ($T_{tQ.i.}$) was between 0.38 and 3.27 mm day^{-1}, with a mean of 0.83 mm day^{-1} and a standard deviation (SD) of 0.77 mm day^{-1} (for 30,671 *Q.i.* trees in the catchment). In the case of *Q.p.*, the scaled-up canopy-normalised transpiration ($T_{tQ.p.}$) was between 0.59 and 3.60 mm day^{-1}, with a mean of 1.19 mm day^{-1} and an SD of 0.85 mm day^{-1} (for 153,757 *Q.p.* trees in the catchment). The larger T_t of *Q.p.* was due to generally more significant influence in Eq. (8) of the higher J_p in *Q.p.* as compared to the higher A_x/A_c ratio in *Q.i.*.

Considering *Q.p.*, our $T_{tQ.p.}$ measurement-range (0.59–3.60 mm day^{-1}) was similar but with a higher minimum and maximum than the ones of the study of Hernández-Santana et al. (2008a) (0.2–3.2 mm day^{-1}), in a Mediterranean mountain forest approximately 200 km south of the Sardón catchment. The difference in $T_{tQ.p.}$ could probably be related to different environmental conditions characterized by more humid climatic conditions with rainfall of ~1000 mm year^{-1} as compared to ~500 mm year^{-1} in the Sardón study area. However, it is also likely that Hernández-Santana et al. (2008a) underestimated their sap flow measurements using TDP method because the TDP does not allow to detect night flow whenever it occurs regularly at night, as it was the case of all measurements in *Q.p.* trees described by Reyes-Acosta and Lubczynski (2012).

The remote-sensing-based, scaled-up dry-season tree transpiration at the 1 ha stand scale (T_{sta}) ranged from 0 to 0.471 mm day^{-1} across the catchment (Fig. 8a); the catchment scale dry-season

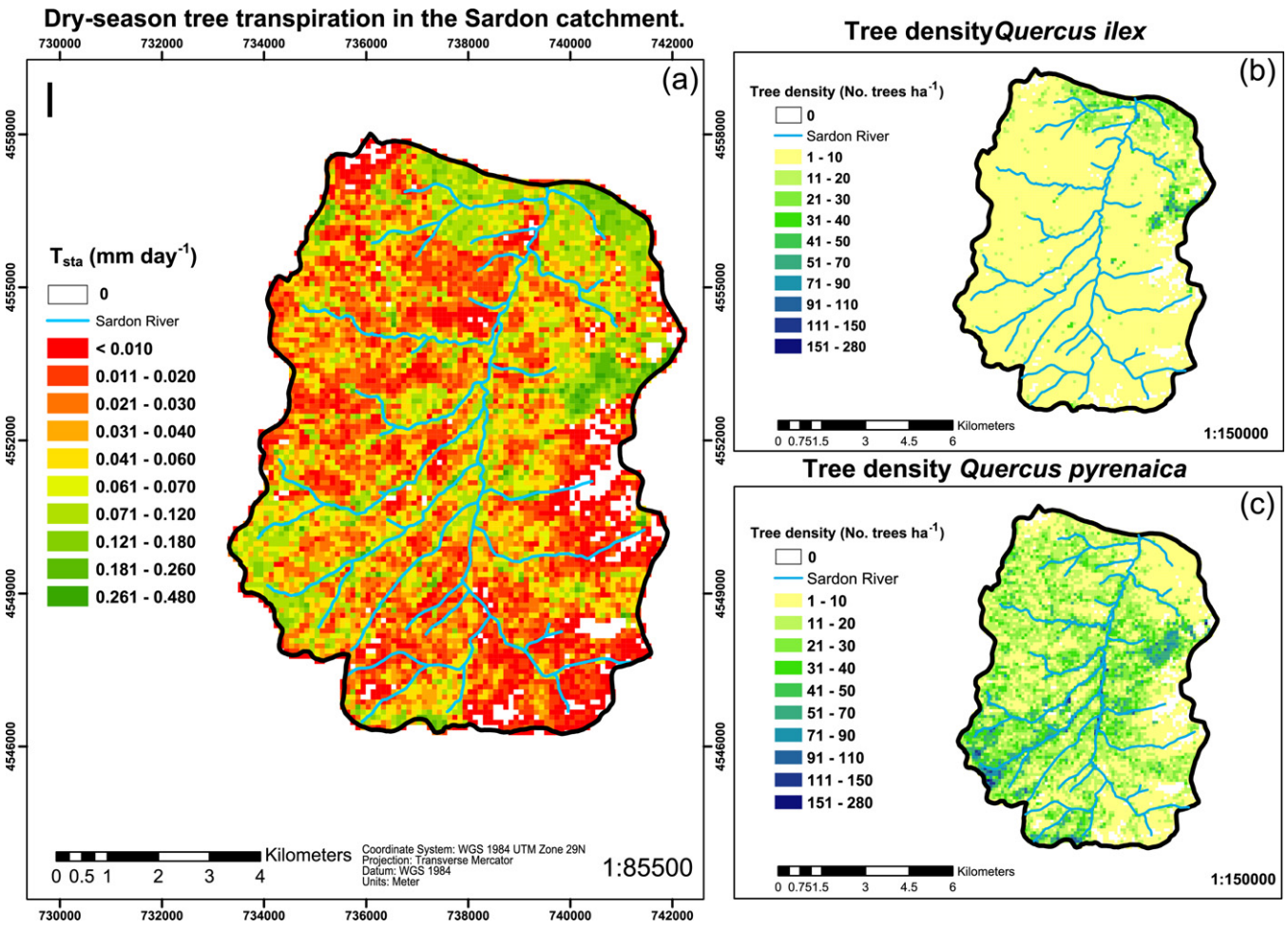

Fig. 8. Tree transpiration and tree density per hectare for *Q.i.* and *Q.p.* species: (a) dry-season tree transpiration in the Sardón catchment at 1 ha stand resolution (T_{sta}) scaled up from remotely sensed images; (b) Sardón catchment *Q.i.* tree density; and (c) Sardón catchment *Q.p.* tree density.

tree transpiration (T_c) was 0.045 mm day^{-1} (average of T_{sta} for the whole catchment) with a standard deviation of 0.041 mm day^{-1}. From the obtained T_c, *Q.i.* and *Q.p.* trees contributed 21% and 79%, respectively. The higher contribution of *Q.p.* trees to dry-season T_c is driven mainly by the greater number of *Q.p.* trees per hectare (average 19 trees ha^{-1}) than *Q.i.* trees (average 4 trees ha^{-1}). The T_{sta} varied widely across the catchment as indicated in Fig. 8 and by the SD of T_c ($T_c \approx SD$). That variability was obviously proportional to tree density. The highest transpiration fluxes were primarily located closer to the stream valleys where tree density was the highest resulting in T_{sta} ranging between 0.181 and 0.480 mm day^{-1}. The areas outside valleys had typically T_{sta} between 0.011 and 0.040 mm day^{-1}.

Fig. 8b and c shows respectively *Q.i.* and *Q.p.* spatial variations of tree densities. *Q.i.* trees dominated only at the north-eastern side of the catchment, far from the streams and river valleys (Fig. 8b). The spatial distribution of *Q.i.* trees suggests that this species is more abundant in locations with relatively deep water table (i.e. far from streams and valleys), because it can overcome water-stress during the dry-season due to its deep root system that is hydraulically connected to deep water sources. In such locations, *Q.i.* trees can maintain a conservative water-use strategy with a quasi-constant water supply from deep sources when the top soil is dry (David et al., 2007), a strategy typical for this species (Mediavilla and Escudero, 2003). In contrast, *Q.p.* trees were abundant in the river valleys and in the south-western part of the catchment (Fig. 8c), i.e. in locations where soil moisture availability and/or water table was close to the surface throughout the dry season (confirmed by soil moisture profiles measured during 2009), allowing them to use a non-conservative water-use strategy and cope with the typically high transpiration demands as previously described by Hernández-Santana et al. (2008a) and Moreno et al. (2011).

Interestingly, T_{sta} was the highest in the north-eastern areas, where *Q.i.* trees dominated (Fig. 8a and b), even though the mean measured sap flux density (J_p) for *Q.i.* trees was lower than that of *Q.p.* trees (Fig. 2 and Table 1). This was because: the BUF used for remote-sensing-based scaling up was steeper for *Q.i.* trees (Fig. 7b) than for *Q.p.* trees (Fig. 7d) resulting in larger A_x for given A_c, and also because *Q.i.* trees in that area are numerous, old and large, so their individual water uptakes are also large due to their higher A_x areas.

A cross-reference of this study with the research of Balugani et al. (2011) on the dry season actual evapotranspiration (ET_a) measured from an Eddy-covariance flux tower carried out in the same Sardón study area was made. It showed that the dry-season tree transpiration within the footprint of the tower (T_f = 0.036 mm day^{-1}), scaled up with the same BUF as in this study, was comparable with the scaled-up catchment transpiration (T_c = 0.045 mm day^{-1}) but represented only 6% of ET_a (0.6 mm day^{-1}). Such low T_f and T_c as compared to ET_a was likely related to: (a) the low tree-density and vegetation cover of *Q.i.* and *Q.p.* trees (the average canopy coverage under the Eddy-covariance foot print and in the catchment was ≈7%, implying low T_{sta}); (b) the location of the eddy tower which was in an area where T_{sta}

Table 5
Comparison between stand-scale and remote-sensing scaling-up techniques of T_{sta} at a 1 ha stand, using biometric ground measurements. *DBH* – diameter at breast height (≈1.3 m), A_c – canopy projected area, A_x – sapwood area and Q_s – sap flow.

Tree species in the stand	*DBH* (m)	A_c (m^2)	A_x (cm^2)	Remote-sensing scaling-up (Q_s) (L day^{-1})	Stand-scale scaling-up (Q_s) (L day^{-1})	Absolute error (AE) (L day^{-1})	Squared error (SE) (L day^{-1})
1 *Q.i.*	1.16	183.96	1633	73.95	68.21	5.74	32.95
2 *Q.i.*	0.80	122.76	1123	50.75	49.09	1.66	2.76
3 *Q.i.*	0.75	113.45	1048	47.34	46.08	1.26	1.59
4 *Q.p.*	0.54	81.36	565	51.92	51.25	0.67	0.45
5 *Q.i.*	0.52	75.24	727	32.73	32.65	0.08	0.01
6 *Q.p.*	0.44	64.08	451	60.23	60.36	0.13	0.02
7 *Q.i.*	0.43	59.40	595	26.73	26.87	0.14	6.02
8 *Q.p.*	0.40	59.04	418	29.55	29.58	0.03	0.01
9 *Q.p.*	0.31	43.92	319	19.49	19.71	0.22	0.05
10 *Q.i.*	0.31	40.32	437	31.27	31.35	0.08	0.01
11 *Q.i.*	0.30	38.52	422	18.81	19.03	0.22	0.05
12 *Q.i.*	0.22	24.48	305	13.49	13.61	0.12	0.01
13 *Q.p.*	0.15	16.56	140	13.20	13.67	0.47	0.22
Total stand (L day^{-1})	n/a	n/a	n/a	469.4	461.4		
Total stand (mm day^{-1})	n/a	n/a	n/a	0.047	0.046		
Mean AE						0.83	
Root mean SE							1.71

was low due to the small size of the canopies (A_c); and (c) a shallow water-table (5 m) in the foot-print area, so that direct bare-soil evaporation of groundwater likely made a larger contribution to ET_a than T_c (Balugani et al., 2011).

The tree-population structure of the Sardón catchment, with an average tree density of ≈19 trees ha^{-1}, is lower than typical Mediterranean woodlands (30–60 trees ha^{-1}) (Carreiras et al., 2006; David et al., 2004; Moreno et al., 2005), but not uncommon (Carreiras et al., 2006; Smit et al., 2008). The observed spatial patterns suggest a division of ecological niches (e.g. distribution of resources and potential competitors) between *Q.i.* and *Q.p.* species, which is likely to decrease inter-specific competition (i.e. between species) for limiting resources, in this case soil water availability. This conclusion is further supported by the fact that in the catchment both species are not found in mixed clusters and rarely close to each other. Human intervention may be another factor shaping the current structure and distribution of vegetation in the Sardón catchment. Human activities can, indeed, be considered to have an impact on the trees, since farming practices in the area are focused on protecting and facilitating conditions favourable for *Q.i.* trees, due to their socio-economic role for pig-grazing under the trees (such pigs are used for the production of "Bellota iberico" ham). In contrast, *Q.p.* trees are relatively less-managed and have no particular economic use in the region, they are sometimes pruned for ornamental reasons or used as fuel. One last, indirect factor that has been reported to affect populations of *Q.i.* species is grazing intensity, which may not allow normal recruitment of seedlings (Smit et al., 2008). However, this factor has a higher effect at local scales than that of the catchment level, where water availability in dry seasons, is the most important factor explaining species distribution in semi-arid areas (Porporato et al., 2001).

3.6. Comparison of remote-sensing and stand scale scaling up

The analysed 1 ha stand contained 8 *Q.i.* and 5 *Q.p.* trees of varying sizes (see Table 5); all trees had been biometrically surveyed. The stand-scale scaling up of the selected area resulted in a T_{sta} value of 0.047 mm day^{-1}, or 469.4 l day^{-1}, while remote-sensing-based scaling up of the same stand 0.046 mm day^{-1} or 461.4 l day^{-1} (see Table 5). Despite lower amount of trees in the analyzed stand (13) than the catchment mean (17), the estimated with both methods T_{sta} were slightly larger than the catchment mean T_{sta} (0.04 ± 0.04 mm day^{-1}). This was because the trees in the selected stand were generally larger than the mean size trees in the catchment. When using the mean absolute error (MAE) and root mean squared error (RMSE) to compare both techniques, it was found that MAE was 0.83 l day^{-1} while RMSE was 1.71 l day^{-1}. These results indicate that differences between upscaling techniques were very low (<2%). The small differences between the two scaling up techniques can be explained by generally higher R^2 found for the *DBH* – A_x BUF (applied to the stand-scale scaling up) than the R^2 for the A_c vs. A_x BUF (applied to the remote-sensing-based scaling up), and due to the eventual errors in the delineation of the canopies from the remotely sensed images. Nevertheless, the comparison between scaling up methods indicated a strong agreement in the T_{sta} calculations at the stand scale, underlining the potential of using spatial imagery of high resolution for scaling-up sap-flow in future studies.

3.7. Uncertainty analysis of remote-sensing-based scaling up

It is important to first clarify that species-specific T_c referred to in this section (T_{cs}) is an abstract term that does not have hydrological meaning, but it is used to represent transpiration contributions of each species spatially. The species-specific T_{cs} was calculated by dividing the sum of all tree sap flows of the particular tree species by the stand area, and then by averaging the values across the 1 ha-resolution grid for the whole catchment.

The assessment of the uncertainty after 1000 Monte-Carlo iterations showed that the combined effect of the species classification errors and the errors in the BUFs resulted in an average T_{cs} of 0.012 mm day^{-1} (*SD* <0.001 mm day^{-1}) for *Q.i.* trees and an average T_{cs} of 0.032 mm day^{-1} (*SD* <0.001 mm day^{-1}) for *Q.p.* trees (Fig. 9a and b). In the case of T_{cs} for all trees in the catchment, it was in average 0.044 mm day^{-1} (*SD* <0.001 mm day^{-1}) (Fig. 9c). The average T_{cs} for *Q.i.* and for *Q.p.* trees were not significantly different as compared with the T_c, for which the error was considered negligible due to the optimisation routine used for reducing J_p measuring errors in the field.

Two factors explain the non-significant difference between the T_{cs} values of the uncertainty analysis and the initial estimations of T_c. First, the "User's" accuracy of the classification map indicated that at least 12% of *Q.p.* trees were in fact *Q.i.* trees, thus, during the Monte-Carlo simulations, ≈18,000 trees (out of 153,757) were added to the T_{cs} calculation for *Q.i.* trees. Second, at least 4% of the *Q.i.* trees were in fact *Q.p.* trees, thus ≈1000 trees (out of 30,671)

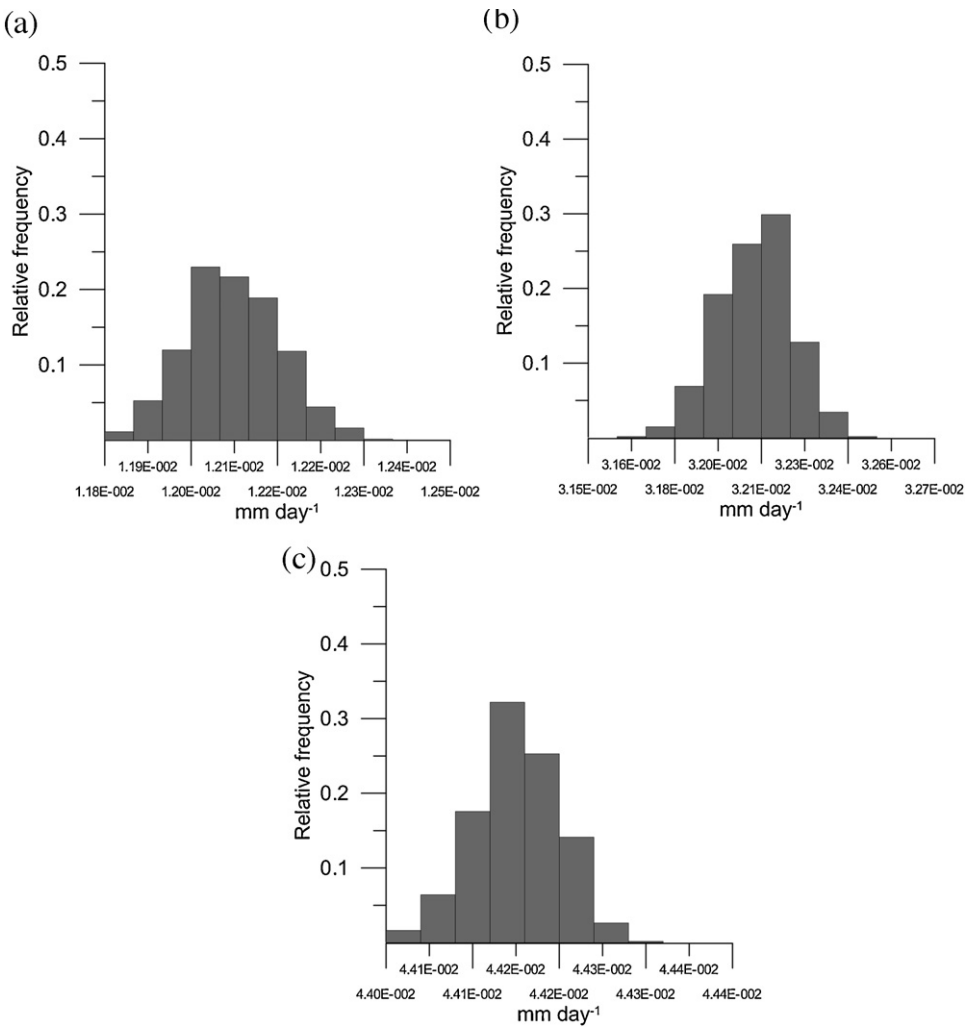

Fig. 9. Relative frequency distribution of the transpiration at the catchment level (T_c) obtained from Monte-Carlo simulations (1000 iterations) of the RUS technique: (a) *Q.i.* trees; (b) *Q.p.* trees; and (c) for both species (all trees in the catchment).

were added to the T_{cs} calculation for *Q.p.* trees. The combination of both factors created a compensation effect that was observed during the simulations. When the number of *Q.p.* trees was reduced, the number of *Q.i.* trees increased, thus increasing T_{cs}, and vice versa. Therefore, as the error in the *Q.p.* classification was higher than for the *Q.i.* classification, and because *Q.p.* had more trees in the catchment, the average T_c obtained from the uncertainty analysis (for 1000 iteration) was slightly, but not significantly, lower than the T_c without any accounting for uncertainty (fewer *Q.p.* trees lead to a lower T_c).

The T_c simulations converged to specific values (Fig. 9), which is confirmed by their low SD, thus indicating that the combination of errors in the classification map and the BUFs had only a slight effect on the estimation of transpiration (<1%). This demonstrates that the assessed uncertainty for the remote-sensing-based scaling up was not significant, confirming the robustness of the estimations for sparse oak-woodlands of the the Sardón catchment.

It is important to note that the proposed method was applied to dry season-tree transpiration assessment, but if there is appropriate sap flow data available, it can be used for wet conditions with comparable uncertainties. As the accuracy of the proposed scaling-up procedure does not depend on the season assessed, but on the accuracy of sap flow measurements together with the accuracy of the scaling-up procedure, no difference of uncertainty across seasons is expected.

4. Conclusions

In this study we proposed a method for mapping dry-season tree transpiration by scaling up sap flow measurements using object attributes identified on high-resolution remotely sensed satellite images. The method here described is novel and more advanced than previous applications because of the following: (1) we introduced in the scaling-up protocol radial and azimuthal sap flow measurements; (2) we assigned sap flow magnitudes of individual trees by categorizing sap-flux densities with respect to the sapwood area, thus enhancing the accuracy of the scaled up estimation; (3) in the scaling up procedure, instead of considering whole sapwood areas for sap-flow calculations, we considered flows of individual sapwood annuli to enhance the precision of the estimations; (4) for defining the attributes of the vegetation spatially in the scaling up procedure, we used a combination of two high resolution multispectral images (QuickBirs and World View II) acquired in two different growing seasons; and (5) finally we provided a Monte-Carlo uncertainty estimations of the procedure.

Through the scaling up of transpiration and the artificial neural-networks (ANNs) simulations we discovered that the tree transpiration in the studied oak woodland ("dehesa") was low $\sim$0.04 mm day^{-1} ($\pm$0.04) and changed minimally throughout the dry season. Furthermore, we found large spatial variability of tree transpiration (T_{sta} spatial patterns), mainly determined by the

density of the *Q.i.* and *Q.p.* tree species constrained by the water availability either as soil moisture or shallow groundwater. This spatial variability information bears an important potential to understand the eco-hydrological role of the *Q.i.* and *Q.p.* species and to promote adequate water management practices in semi-arid areas, such as as the Sardón catchment.

Transpiration mapping by remote sensing scaling up of sap flow measurements is a convenient tool for understanding the hydrological dynamics of the plant-soil-water interactions but also for quantitative estimates of plant water uptake in future studies.

Acknowledgements

We would like to thank Prof. Jan Čermák for his comments and support in the earlier versions of this manuscript. We also want to thank Dr. D.G. Rossiter for his valuables contributions in the implementation of the uncertainty-analysis, Dr. Yussif Hussin for his valuable comments on the classification accuracy assessment, the hydrological-resources team of the CIALE institute at the Salamanca University for their logistic support, Chandra Prasad Ghimire and Enrico Balugani for their support in the field campaigns and the manuscript writing. Finally, we want to extend our appreciation to the two anonymous reviewers.

References

Abramowitz, G., 2005. Towards a benchmark for land surface models. Geophys. Res. Lett. 32, L22702.

Allen, R., Pereira, L., Raes, D., Smith, M., 1998. Crop Evapotranspiration-Guidelines for Computing Crop Water Requirements-FAO Irrigation and Drainage Paper 56, vol. 300. FAO, Rome.

Baatz, M., Benz, U., Dehghani, S., Heynen, M., Holtje, A., Hofmann, P., Lingenfelder, I., Mimler, M., Sohlbach, M., Weber, M., 2001. Ecognition object oriented image analysis. User Guide. Definiens Imaging, Mnchen, Germany.

Balugani, E., Reyes-Acosta, J.L., van der Tol, C., Francs, A.P., Lubczynski, M.W., 2011. Partitioning and sourcing of dry season evapotranspiration fluxes at the footprint of the eddy covariance tower in sardn semi-arid location in Spain. In: ZNS Conference Proceedings.

Boegh, E., Soegaard, H., Hanan, N., Kabat, P., Lesch, L., 1999. A remote sensing study of the ndvits relationship and the transpiration from sparse vegetation in the sahel based on high-resolution satellite data. Remote Sens. Environ. 69, 224–240.

Brown, A.E., Zhang, L., McMahon, T.A., Western, A.W., Vertessy, R.A., 2005. A review of paired catchment studies for determining changes in water yield resulting from alterations in vegetation. J. Hydrol. 310, 28–61.

Calder, I.R., 1978. Transpiration observations from a spruce forest and comparisons with predictions from an evaporation model. J. Hydrol. 38, 33–47.

Carreiras, J.M.B., Pereira, J.M.C., Pereira, J.S., 2006. Estimation of tree canopy cover in evergreen oak woodlands using remote sensing. Forest Ecol. Manage. 223, 45–53.

Caspari, H.W., Green, S.R., Edwards, W.R.N., 1993. Transpiration of well-watered and water-stressed asian pear trees as determined by lysimetry, heat-pulse, and estimated by a Penman–Monteith model. Agric. Forest Meteorol. 67, 13–27.

Čermák, J., Kučera, J., 1990. Scaling up transpiration data between trees, stands and watersheds. Silva Carelica 15, 101–120.

Čermák, J., Kučera, J., Nadezhdina, N., 2004. Sap flow measurements with some thermodynamic methods, flow integration within trees and scaling up from sample trees to entire forest stands. Trees Struct. Funct. 18, 529–546.

Čermák, J., Ulehla, J., Kučera, J., Penka, M., 1982. Sap flow rate and transpiration dynamics in the full-grown oak (quercus robur l.) in floodplain forest exposed to seasonal floods as related to potential evapotranspiration and tree dimensions. Plant Biol. 24, 446–460.

Chavarro, R.D.C., Rossiter, D., Lubczynski, M., 2009. Transpiration mapping from upscaled sapflow. ITC, University of Twente, Enschede, The Netherlands.

Chu, C.R., Hsieh, C.I., Wu, S.Y., Phillips, N.G., 2009. Transient response of sap flow to wind speed. J. Exp. Bot. 60, 249–255.

Cienciala, E., Kucera, J., Malmer, A., 2000. Tree sap flow and stand transpiration of two acacia mangium plantations in sabah, borneo. J. Hydrol. 236, 109–120.

Cohen, J., 1960. A coefficient of agreement for nominal scales. Educ. Psychol. Measure. 20, 37–46.

Congalton, R., 1996. Accuracy assessment: a critical component of land cover mapping. In: Scott, J.M., Tear, T.H., Davis, F.W. (Eds.), Gap Analysis: A Landscape Approach to Biodiversity Planning. American Society for Photogrammetry and Remote Sensing, Bethesda, Maryland, US, pp. 119–131.

Congalton, R.G., 1991. A review of assessing the accuracy of classifications of remotely sensed data. Remote Sens. Environ. 37, 35–46.

Congalton, R.G., Green, K., 1999. Assessing the accuracy of remotely sensed data: principles and practices. PBD: 1999. Lewis Publishers, Boca Raton, FL, USA.

Corcuera, L., Camarero, J., Gil-Pelegrn, E., 2004. Effects of a severe drought on quercus ilex radial growth and xylem anatomy. Trees Struct. Funct. 18, 83–92.

Cristóbal, J., Poyatos, R., Ninyerola, M., Llorens, P., Pons, X., 2011. Combining remote sensing and gis climate modelling to estimate daily forest evapotranspiration in a mediterranean mountain area. Hydrol. Earth Syst. Sci. 15, 1563.

David, T.S., Ferreira, M.I., Cohen, S., Pereira, J.S., David, J.S., 2004. Constraints on transpiration from an evergreen oak tree in southern Portugal. Agric. Forest Meteorol. 122, 193–205.

David, T.S., Henriques, M.O., Kurz-Besson, C., Nunes, J., Valente, F., Vaz, M., Pereira, J.S., Siegwolf, R., Chaves, M.M., Gazarini, L.C., David, J.S., 2007. Water-use strategies in two co-occurring mediterranean evergreen oaks: surviving the summer drought. Tree Physiol. 27, 793–803.

Devitt, D., Berkowitz, M., Schulte, P., Morris, R., 1993. Estimating transpiration for three woody ornamental tree species using stem-flow gauges and lysimetry. HortScience 28, 320.

Do, F., Rocheteau, A., 2002a. Influence of natural temperature gradients on measurements of xylem sap flow with thermal dissipation probes. 1. Field observations and possible remedies. Tree Physiol. 22, 641–648.

Do, F., Rocheteau, A., 2002b. Influence of natural temperature gradients on measurements of xylem sap flow with thermal dissipation probes. 2. advantages and calibration of a noncontinuous heating system. Tree Physiol. 22, 649–654.

Dorren, L.K.A., Maier, B., Seijmonsbergen, A.C., 2003. Improved landsat-based forest mapping in steep mountainous terrain using object-based classification. Forest Ecol. Manage. 183, 31–46.

Ehlers, M., Gahler, M., Janowsky, R., 2003. Automated analysis of ultra high resolution remote sensing data for biotope type mapping: new possibilities and challenges. ISPRS J. Photogramm. Remote Sens. 57, 315–326.

Ford, C.R., Hubbard, R.M., Kloeppel, B.D., Vose, J.M., 2007. A comparison of sap flux-based evapotranspiration estimates with catchment-scale water balance. Agric. Forest Meteorol. 145, 176–185.

Gea-Izquierdo, G., Martn-Benito, D., Cherubini, P., Caellas, I., 2009. Climate-growth variability in quercus ilex l. West iberian open woodlands of different stand density. Ann. For. Sci. 66, 802.

Giles, M.F., 2002. Status of land cover classification accuracy assessment. Remote Sens. Environ. 80, 185–201.

Granier, A., 1985. Une nouvelle méthode pour la mesure du flux de sève brute dans le tronc des arbres. Ann. Sci. For. 42, 193–200.

Granier, A., 1987. Evaluation of transpiration in a douglas-fir stand by means of sap flow measurements. Tree Physiol. 3, 309–320.

Granier, A., Anfodillo, T., Sabatti, M., Cochard, H., Dreyer, E., Tomasi, M., Valentini, R., Breda, N., 1994. Axial and radial water flow in the trunks of oak trees: a quantitative and qualitative analysis. Tree Physiol. 14, 1383–1396.

Granier, A., Biron, P., Köstner, B., Gay, L.W., Najjar, G., 1996. Comparisons of xylem sap flow and water vapour flux at the stand level and derivation of canopy conductance for scots pine. Theor. Appl. Climatol. 53, 115–122.

Hatton, T.J., Wu, H.I., 1995. Scaling theory to extrapolate individual tree water use to stand water use. Hydrol. Processes 9, 527–540, http://dx.doi.org/10.1002/hyp.3360090505.

Hay, A., 1979. Sampling designs to test land-use map accuracy. Photogramm. Eng. Rem. Sens., 45.

Hernández-Santana, V., David, T.S., Martínez-Fernández, J., 2008a. Environmental and plant-based controls of water use in a mediterranean oak stand. Forest Ecol. Manage. 255, 3707–3715.

Hernández-Santana, V., Martínez-Fernández, J., Morán, C., Cano, A., 2008b. Response of quercus pyrenaica (melojo oak) to soil water deficit: a case study in spain. Eur. J. Forest Res. 127, 369–378.

Hernández-Santana, V., Martínez-Vilalta, J., Martínez-Fernández, J., Williams, M., 2009. Evaluating the effect of drier and warmer conditions on water use by quercus pyrenaica. Forest Ecol. Manage. 258, 1719–1730.

Janssen, L., Huurneman, G., Bakker, W., Reeves, C., Gorte, B., Pohl, C., Weir, M., Horn, J., Prakash, A., Woldai, T., 2001. Principles of Remote Sensing: An Introductory Textbook. Volume 2 of ITC Educational Textbook Series, second ed. ITC, Enschede.

Kimani, J., Hussin, Y., Lubczynski, M.W., Chavarro, D., Obakeng, O., 2007. Mapping savannah trees in kalahari using high resolution remotely sensed images and object-oriented classification. Int. J. Geoinformatics 3.

Köstner, B., Granier, A., Cermak, J., 1998. Sapflow measurements in forest stands: methods and uncertainties. Ann. Sci. For. 55, 13–27.

Kumagai, T., Nagasawa, H., Mabuchi, T., Ohsaki, S., Kubota, K., Kogi, K., Utsumi, Y., Koga, S., Otsuki, K., 2005. Sources of error in estimating stand transpiration using allometric relationships between stem diameter and sapwood area for cryptomeria japonica and chamaecyparis obtusa. For. Ecol. Manage. 206, 191–195.

Liu, X., Kang, S., Li, F., 2009. Simulation of artificial neural network model for trunk sap flow of pyrus pyrifolia and its comparison with multiple-linear regression. Agric. Water Manage. 96, 939–945.

Lu, P., Urban, L., Zhao, P., 2004. Granier's thermal dissipation probe (tdp) method for measuring sap flow in trees: Theory and practice. Acta Bot. Sin. 46, 631–646.

Lu, P., Woo, K.C., Liu, Z.T., 2002. Estimation of whole-plant transpiration of bananas using sap flow measurements. J. Exp. Bot. 53, 1771–1779 http://jxb.oxfordjournals.org/content/53/375/1771.full.pdf+html

Lubczynski, M., Gurwin, J., 2005. Integration of various data sources for transient groundwater modeling with spatio-temporally variable fluxes-sardon study case, Spain. J. Hydrol. 306, 71–96.

Lubczynski, M.W., 2000. Groundwater evapotranspiration, underestimated component of the groundwater balance in a semi – arid environment. Serowe Case, Botswana, Rotterdam.
Lubczynski, M.W., 2009. The hydrogeological role of trees in water-limited environments. Hydrogeol. J. 17, 247–259.
Lubczynski, M.W., Chavarro-Rincon, D., Roy, J., 2012. Novel, cyclic heat dissipation method for the correction of natural temperature gradients in sap flow measurements. Part 1. Theory and application. Tree Physiol.
Lundblad, M., Lindroth, A., 2002. Stand transpiration and sapflow density in relation to weather, soil moisture and stand characteristics. Basic Appl. Ecol. 3, 229–243.
Manes, F., Vitale, M., Donato, E., Giannini, M., Puppi, G., 2006. Different ability of three mediterranean oak species to tolerate progressive water stress. Photosynthetica 44, 387–393.
Martínez-Vilalta, J., nol, J.P., Beven, K., 2002. A hydraulic model to predict drought-induced mortality in woody plants: an application to climate change in the mediterranean. Ecol. Model. 155, 127–147.
McCuen, R., Knight, Z., Cutter, A., 2006. Evaluation of the nashsutcliffe efficiency index. J. Hydrol. Eng. 11, 597.
Mediavilla, S., Escudero, A., 2003. Stomatal responses to drought at a mediterranean site: a comparative study of co-occurring woody species differing in leaf longevity. Tree Physiol. 23, 987–996.
Moore, D.J.P., Hu, J., Sacks, W.J., Schimel, D.S., Monson, R.K., 2008. Estimating transpiration and the sensitivity of carbon uptake to water availability in a subalpine forest using a simple ecosystem process model informed by measured net CO_2 and H_2O fluxes. Agric. Forest Meteorol. 148, 1467–1477.
Moreno, G., Gallardo, J.F., Vicente, M.n., 2011. How mediterranean deciduous trees cope with long summer drought? the case of quercus pyrenaica forests in western spain. In: Bredemeier, M., Cohen, S., Godbold, D.L., Lode, E., Pichler, V., Schleppi, P., Heldmaier, G., Jackson, R.B., Lange, O.L., Mooney, H.A., Schulze, E.D., Sommer, U. (Eds.), In: Forest Management and the Water Cycle, vol. 212. Springer, Netherlands, pp. 187–201.
Moreno, G., Obrador, J.J., Cubera, E., Dupraz, C., 2005. Fine root distribution in dehesas of central-western Spain. Plant Soil 277, 153–162.
Murray, R.S., Nagler, P.L., Morino, K., Glenn, E.P., 2009. An empirical algorithm for estimating agricultural and riparian evapotranspiration using modis enhanced vegetation index and ground measurements of et. ii. Application to the lower colorado river, U.S. Remote Sens. 1, 1125–1138.
Nadezhdina, N., Čermák, J., Ceulemans, R., 2002. Radial patterns of sap flow in woody stems of dominant and understory species: scaling errors associated with positioning of sensors. Tree Physiol. 22, 907–918.
Nadezhdina, N., Vandegehuchte, M., Steppe, K., 2012. Sap flux density measurements based on the heat field deformation method. Trees 26, 1439–1448.
Nadezhdina, N.J., Čermaák, Nadezhdin, V., 1998. The heat field deformation method for sap flow measurement. In: Crmak, J., Nadezhdina, N. (Eds.), Proc 4th Int Workshop, Zidlochovice, C.R.I.P.B. (Ed.), 4th International Workshop on Measuring Sap flow in Intact Plants. , p. 7292.
Nagler, P., Jetton, A., Fleming, J., Didan, K., Glenn, E., Erker, J., Morino, K., Milliken, J., Gloss, S., 2007. Evapotranspiration in a cottonwood (populus fremontii) restoration plantation estimated by sap flow and remote sensing methods. Agric. Forest Meteorol. 144, 95–110.
O'Brien, J.J., Oberbauer, S.F., Clark, D.B., 2004. Whole tree xylem sap flow responses to multiple environmental variables in a wet tropical forest. Plant Cell Environ. 27, 551–567.
Paço, T.A., David, T.S., Henriques, M.O., Pereira, J.S., Valente, F., Banza, J., Pereira, F.L., Pinto, C., David, J.S., 2009. Evapotranspiration from a mediterranean evergreen oak savannah: The role of trees and pasture. J. Hydrol. 369, 98–106.
Porporato, A., Laio, F., Ridolfi, L., Rodriguez-Iturbe, I., 2001. Plants in water-controlled ecosystems: active role in hydrologic processes and response to water stress: Iii. vegetation water stress. Adv. Water Resour. 24, 725–744.
Poyatos, R., Cermak, J., Llorens, P., 2007. Variation in the radial patterns of sap flux density in pubescent oak (quercus pubescens) and its implications for tree and stand transpiration measurements. Tree Physiol. 27, 537–548.
Quinn, G.P., Keough, M.J., 2002. Experimental Design and Data Analysis for Biologists. Cambridge University Press, Cambridge, UK.
Regalado, C., Ritter, A., Aschan, G., 2009. Tdp measurements to determine nighttime sap-flow and the impact of fog in tree transpiration of a laurisilva forest. Acta Hort. (ISHS) 846, 367–374.
Reyes-Acosta, J.L., Lubczynski, M.W., 2012. Optimization of dry-season sap flow measurements in an oak semi-arid open woodland in spain. Ecohydrology, Early online view.
Reyes-Acosta, J.L., Vandegehuchte, M.W., Steppe, K., Lubczynski, M.W., 2012. Novel, cyclic heat dissipation method for the correction of natural temperature gradients in sap flow measurements. Part 2. Laboratory validation. Tree Physiol. 32, 913–929.
Rice, J., 2006. Mathematical statistics and data analysis. Thomson Learn.
Ritter, A., Muoz-Carpena, R., Regalado, C., 2011. Capacidad de prediccin de modelos aplicados a la zs: herramienta informtica para la adecuada evaluacin de la bondad-de-ajuste con significacin estadstica. In: Fernndez, J., Martin, N.S. (Eds.), Estudios en la zona no saturada del suelo: ZNS11. Universidad de Salamanca, Salamanca, pp. 259–264.
Smit, C., den Ouden, J., Daz, M., 2008. Facilitation of quercus ilex recruitment by shrubs in mediterranean open woodlands. J. Veg. Sci. 19, 193–200.
Stehman, S.V., Czaplewski, R.L., 1998. Design and analysis for thematic map accuracy assessment: fundamental principles. Remote Sens. Environ. 64, 331–344.
Stöhr, A., Lösch, R., 2004. Xylem sap flow and drought stress of fraxinus excelsior saplings. Tree Physiol. 24, 169–180.
Story, M., Congalton, R., 1986. Accuracy assessment: a user's perspective. Photogramm. Eng. Remote Sens. 52, 397–399.
Verbeeck, H., Steppe, K., Nadezhdina, N., Op de Beeck, M., Deckmyn, G., Meiresonne, L., Lemeur, R., Cermak, J., Ceulemans, R., Janssens, I.A., 2007. Stored water use and transpiration in scots pine: a modeling analysis with anafore. Tree Physiol. 27, 1671–1685.
Vertessy, R.A., Hatton, T.J., Reece, P., O'Sullivan, S.K., Benyon, R.G., 1997. Estimating stand water use of large mountain ash trees and validation of the sap flow measurement technique. Tree Physiol. 17, 747–756.
Wheeler, T.D., Stroock, A.D., 2008. The transpiration of water at negative pressures in a synthetic tree. Nature 455, 208–212.
Whitley, R., Medlyn, B., Zeppel, M., Macinnis-Ng, C., Eamus, D., 2009. Comparing the Penman–Monteith equation and a modified jarvisstewart model with an artificial neural network to estimate stand-scale transpiration and canopy conductance. J. Hydrol. 373, 256–266.
Williams, M., Bond, B., Ryan, M., 2001. Evaluating different soil and plant hydraulic constraints on tree function using a model and sap flow data from ponderosa pine. Plant Cell Environ. 24, 679–690.
Wullschleger, S.D., Meinzer, F.C., Vertessy, R.A., 1998. A review of whole-plant water use studies in trees. Tree Physiol. 18, 499–512.
Zeppel, M.J.B., Murray, B.R., Barton, C., Eamus, D., 2004. Seasonal responses of xylem sap velocity to vpd and solar radiation during drought in a stand of native trees in temperate Australia. Funct. Plant Biol. 31, 461–470.